

Efficient Parametrization of the Vertex Function, Ω -Scheme, and the (t, t') -Hubbard Model at Van Hove Filling

Christoph Husemann* and Manfred Salmhofer†
Institut für Theoretische Physik, Universität Heidelberg
D-69124 Heidelberg, Germany
 (January 12, 2009)

Abstract

We propose a new parametrization of the four-point vertex function in the one-loop one-particle irreducible renormalization group (RG) scheme for fermions. It is based on a decomposition of the effective two-fermion interaction into fermion bilinears that interact via exchange bosons. The numerical computation of the RG flow of the boson propagators reproduces the leading weak coupling instabilities of the two-dimensional Hubbard model at Van Hove filling, as they were obtained by a temperature RG flow in [12]. Instead of regularizing with temperature, we here use a soft frequency Ω -regularization that likewise does not artificially suppress ferromagnetism. Besides being more efficient than previous N -patch schemes, this parametrization also reduces the ambiguities in introducing boson fields.

1 Introduction

In the past decade fermionic Wilsonian renormalization group (RG) methods have been very successful in classifying weak coupling instabilities of the two-dimensional (t, t') -Hubbard model [6, 7, 12, 13, 15, 32, 33]. The starting point in these methods is an exact functional equation. Besides being very useful for proving mathematical statements, this equation can be approximated to allow a direct numerical calculation. In the case of weak coupling an expansion in the fermionic fields can be truncated by setting the six-point function to zero. For an appropriate Fermi surface geometry this one-loop approximation is also justified for intermediate couplings and scales [25].

Successes of the fermionic one-loop RG method include the explanation of the interplay of antiferromagnetic and superconducting instabilities in the Hubbard model for small next to nearest neighbor hopping $-t'$. Results were first obtained using Polchinskis version of the RG [32, 33], the Wick ordered scheme [6, 7], and the one-particle irreducible (1PI) scheme [13, 15]. Near half filling, where the Fermi surface is nested, antiferromagnetism was found to be the leading instability. For smaller fillings on the hole doped side, where the Fermi surface is more strongly curved and regular, $d_{x^2-y^2}$ -wave superconductivity is dominating (although not present initially in the repulsive Hubbard model, such a term is generated as an effective interaction in the RG flow; specifically, it is induced by antiferromagnetic correlations).

*c.husemann@thphys.uni-heidelberg.de

†m.salmhofer@thphys.uni-heidelberg.de

In between the two regions the antiferromagnetic and superconducting tendencies mutually reinforce each other [9, 15]. This saddle point regime, where the main contribution comes from the saddle or Van Hove points, is interpreted as the weak coupling analogue of the Mott state, but not yet fully understood.

In all works mentioned in the last paragraph a Fermi surface momentum or frequency cut-off was used. Although being conceptionally clear, this regularization suppresses small-momentum particle-hole fluctuations, as pointed out in [12]. Overcoming this drawback by using temperature as a flow parameter, the leading instability for larger hopping $-t' \in [0.34t, 0.5t]$ was found to be ferromagnetism at Van Hove filling and triplet superconductivity away from Van Hove filling [11, 12]. This result was qualitatively confirmed by the same method in [18], by an interaction RG flow [10], and a two-particle self-consistent Monte Carlo approach [8]. The mutual suppression of ferromagnetic and d -wave superconducting tendencies decreases the critical scale at Van Hove filling for intermediate $-t'$ by several orders of magnitude. Within numerical accuracy, the instability analysis of [11, 12] even suggests the existence of a quantum critical point between the ferromagnet and the superconductor.

The one-loop 1PI RG flow used here is described by the evolution of an effective four-point vertex function and a selfenergy. Even if the selfenergy is not taken into account, the flow equation for the four-point function is a non-linear integro-differential equation (see Section 2). This equation has to be solved for a function with three independent momenta and three independent frequencies. For a numerical computation, as applied by the above mentioned studies, further approximations are needed. By Taylor expansion and power counting it can be argued that the main contribution to low energy excitations comes from frequency zero. All above mentioned one-loop studies neglect the frequency dependence of the vertex function and evaluate the right hand side of the flow equation at frequency zero. In a next step the momentum dependence is discretized. Again by a low energy argument, the momenta of the vertex function are projected onto the Fermi surface in most one-loop studies. In a so-called N -patch scheme [3, 32] the Fermi surface is divided into N patches,¹ and the angular dependence of the vertex on each momentum is approximated by a constant in each patch. Evaluating integrals as sums over patches, this leads to a coupled system of $\sim N^3$ ordinary, non-linear differential equations, which can be solved numerically. In [10] the momentum dependence is not projected onto the Fermi surface, so that full momentum space $(-\pi, \pi)^2$ has to be covered by patches.

Despite the successes of the one-loop N -patch schemes, the method shows room for improvement. – First of all, the selfenergy is neglected in most one-loop RG studies. Quasi particle scattering rates of the Landau Fermi liquid are calculated in [9, 13, 19, 23, 31], which gives a first hint of selfenergy effects. Deformations of the

¹This only applies for $N > 2$. The extreme case are the two-patch models, where, contrary to N -patch schemes, full momentum space is not taken into account. At Van Hove filling they expect the main contribution to come from two small patches around the Van Hove points [4, 15, 18].

Fermi surface due to the real part of the selfenergy are taken into account in [15]. A new dynamical adjustment of the propagator [24] can help to include the selfenergy entirely. – A second problem is the observed flow to strong coupling, which limits the validity of the one-loop RG flow. The flow has to be stopped before all scales are integrated out. That is, the full model is not recovered in the flow since the infrared regularization is not removed completely. This drawback may be overcome with a modified one-loop scheme by allowing the flow to continue in a symmetry broken phase [17, 26]. Using this modified scheme the exact solution of a mean-field model for superconductivity is obtained in the thermodynamic limit [14, 26]. Furthermore, the scheme has been recently applied to the attractive Hubbard model [5]. Due to the emergence of an effective superconducting gap, which regularizes infrared divergencies, all scales can be integrated out. However, since the vertex function is not charge invariant anymore, the flow equations become very complicated. Besides the purely fermionic description of the RG flow, a bosonic continuation with mean-field theory [22] or partially bosonized RG flows [2, 20, 29, 30] are promising methods to treat the symmetry-broken phases.

We also address a third problem of the one-loop N -patch schemes, which is the parametrization of the effective vertex function. Although the initial four-point vertex function of the Hubbard model is a constant in momentum space, a non-trivial and physically important momentum structure evolves in the one-loop RG flow. The approximations entailed by the projections in N -patch schemes are not yet fully understood. A severe restriction on the possible choice of N is the high computational cost of solving $\sim N^3$ ordinary differential equations, whose coefficients have to be calculated as two-dimensional integrals in every integration step. For the same reason, including the frequency dependence is very costly. A more efficient parametrization of the four-point vertex function should identify the relevant processes. Their separation from irrelevant remainders can be guided by previous one-loop studies and the observation that the identification of the leading instabilities is determined by the asymptotic singular structure of the flow equation.

In Section 3 we propose a new parametrization of the vertex function in the one-particle irreducible RG scheme. Guided by the singular momentum structure of the right hand side of the flow equation, we identify three channels with distinct singular momentum structures.² All graphs of the flow equation are uniquely assigned to a channel and the channels are general two-fermion interactions, so this is no approximation. However, since we define the channels based on their singular momentum structure, there are still ambiguities involved. This condition allows different definitions, for example, how a constant term is distributed over the channels. Therefore the initial on-site interaction is not assigned to a channel but kept fixed in the flow explicitly. Nevertheless, the definition of the channels in terms of graphs is natural from the structure of the flow equation.

In the thus defined channels the effective two-fermion interaction is expanded

²In a similar approach the effective vertex function of the single impurity Anderson model was recently written as a sum of three functions, each dependent on only one singular frequency [16].

in terms corresponding to fermion bilinears that interact via exchange bosons. For this study, we choose scale- and frequency-independent form factors for the fermion bilinears. In Section 4, we show that only a small number of terms is needed to capture the essential features of the one-loop RG flow in the case where one channel is dominant. In the case of competing channels, we choose the parametrization guided by the results from N -patch studies. Inserting this decomposition into the RG equation and projecting the right hand side onto the coefficients of the expansions, the flow equations for the boson propagators are derived. In Section 6 we state these flow equations for general expansions with a finite number of form factors when the tails of the expansions are neglected.

We test the proposed parametrization of the vertex function in an application to the (t, t') -Hubbard model at Van Hove filling and temperature zero. Because at this filling, the interplay between superconductivity and ferromagnetism is important, it is essential to choose a scale-dependent regularization that does not artificially suppress small momentum particle-hole fluctuations [12]. Here we do not use the temperature flow, but instead choose a very mild infrared regulator that keeps these fluctuations, but provides enough regularization to have a well-defined flow equation, see Section 5. Further approximations are applied for the numerical implementation in Section 7, where we neglect the frequency dependence of the boson propagators and discretize their momentum dependence using step functions. Since this momentum dependence is mainly determined by the one-loop bubbles, there is good guidance in that. Also, we choose a small number of form factors. The numerical results are stated and discussed in Section 8. We obtain the same ordering tendencies of the Hubbard model at Van Hove filling as in [12].

In the remaining part of this introduction we describe the model and our notations. Consider the two-dimensional quadratic lattice $\Gamma = \mathbb{Z}^2/L\mathbb{Z}^2$ with unit spacing, length $L \in 2\mathbb{N}$, and periodic boundary conditions. Then the dual lattice or momentum space is given by the torus $\Gamma^* = \frac{2\pi}{L}\mathbb{Z}^2/(2\pi\mathbb{Z}^2)$. Let $a_{\mathbf{p},\sigma}$ and $a_{\mathbf{p},\sigma}^\dagger$ be the fermion operators on the associated Fock space with momenta $\mathbf{p} \in \Gamma^*$ and spin $\sigma \in \{+, -\}$ in quantization direction. The (t, t') -Hubbard model on Γ is defined by the Hamiltonian

$$\mathcal{H}[a^\dagger, a] = \sum_{\substack{\mathbf{p} \in \Gamma^* \\ \sigma \in \{+, -\}}} e(\mathbf{p}) a_{\mathbf{p},\sigma}^\dagger a_{\mathbf{p},\sigma} + U \sum_{\mathbf{p}_1 \dots \mathbf{p}_3 \in \Gamma^*} a_{\mathbf{p}_1,+}^\dagger a_{\mathbf{p}_2,-}^\dagger a_{\mathbf{p}_3,-} a_{\mathbf{p}_1+\mathbf{p}_2-\mathbf{p}_3,+} \quad (1)$$

with an on-site repulsion $U > 0$ between electrons. The kinetic term of (1) emerges in a tight binding approximation. That is, the transfer integral, which describes electron hopping between different lattice sites in real space Γ , is set to t for nearest neighbors and $-t'$ for next to nearest neighbors. In momentum space this corresponds to the dispersion relation

$$e(\mathbf{p}) = -2t(\cos p_x + \cos p_y) - 4t' \cos p_x \cos p_y - \mu, \quad (2)$$

where the chemical potential μ is already included in the definition of $e(\mathbf{p})$ and \mathcal{H} , which is convenient for setting up the grand canonical partition function.

In the following t is set to one, that is, all quantities are measured in energy units of t . The next to nearest neighbor hopping is considered in the parameter range $-t' \in (0, \frac{t}{2})$. It determines the shape of the non-interacting Fermi surface together with the chemical potential. For $\mu = 4t'$ the system is at Van Hove filling where the Fermi surface intersects the Van Hove points, where the gradient of the dispersion (2) vanishes. This causes a logarithmic divergence in the density of states.

2 The Fermionic 1PI One-Loop RG

We consider the one-particle irreducible (1PI) fermionic renormalization group (RG) flow in the one-loop approximation [25]. Since we restrict the RG flow to the symmetric phase, the effective interaction, which depends on the RG scale Λ , is assumed to be $SU(2)$ - and $U(1)$ -symmetric, as is the initial Hubbard interaction. An effective two-fermion interaction with those symmetries can be generally written in terms of a four-point vertex function V in the following way

$$\mathcal{V}_\Lambda[\Psi] = \frac{1}{2} \int dp_1 \dots dp_4 \delta(p_1 + p_2 - p_3 - p_4) V_\Lambda(p_1, p_2, p_3) \quad (3)$$

$$\times \sum_{\substack{\sigma, \sigma' \\ \in \{+, -\}}} \bar{\psi}_\sigma(p_1) \bar{\psi}_{\sigma'}(p_2) \psi_{\sigma'}(p_3) \psi_\sigma(p_4).$$

Due to momentum conservation, the four-point vertex function V_Λ is a function of three independent momenta and frequencies. Here we denote $p = (p_0, \mathbf{p})$ with Matsubara frequency p_0 and spatial momentum \mathbf{p} . The integral $\int dp$ is shorthand notation for $\frac{1}{\beta} \sum_{p_0} \int_{(-\pi, \pi]^2} \frac{d^2 \mathbf{p}}{(2\pi)^2}$ in the thermodynamic limit $L \rightarrow \infty$ and at inverse temperature β . The initial on-site interaction of the (t, t') -Hubbard model is characterized by the constant vertex function $V_{\text{H.M.}}(p_1, p_2, p_3) = U$.

The flow equation for the effective vertex function in the 1PI RG scheme reads

$$\dot{V}_\Lambda(p_1, \dots, p_3) = \mathcal{T}_{\text{pp}}(p_1, \dots, p_3) + \mathcal{T}_{\text{ph}}^{\text{d}}(p_1, \dots, p_3) + \mathcal{T}_{\text{ph}}^{\text{cr}}(p_1, \dots, p_3), \quad (4)$$

where the dot denotes the derivative with respect to the scale Λ . The particle-particle contribution and the crossed and direct particle-hole contributions are respectively given by

$$\mathcal{T}_{\text{pp}}(p_1, \dots, p_3) = - \int dp \left[\frac{d}{d\Lambda} G(p) G(p_1 + p_2 - p) \right] V_\Lambda(p_1, p_2, p) V_\Lambda(p_1 + p_2 - p, p, p_3)$$

$$\mathcal{T}_{\text{ph}}^{\text{cr}}(p_1, \dots, p_3) = - \int dp \left[\frac{d}{d\Lambda} G(p) G(p + p_3 - p_1) \right] V_\Lambda(p_1, p + p_3 - p_1, p_3)$$

$$\times V_\Lambda(p, p_2, p + p_3 - p_1)$$

$$\mathcal{T}_{\text{ph}}^{\text{d}}(p_1, \dots, p_3) = \int dp \left[\frac{d}{d\Lambda} G(p) G(p + p_2 - p_3) \right] \left[2V_\Lambda(p_1, p + p_2 - p_3, p) V_\Lambda(p, p_2, p_3) \right.$$

$$- V_\Lambda(p_1, p + p_2 - p_3, p_1 + p_2 - p_3) V_\Lambda(p, p_2, p_3)$$

$$\left. - V_\Lambda(p_1, p + p_2 - p_3, p) V_\Lambda(p, p_2, p + p_2 - p_3) \right].$$

The scale derivatives in the integrands act only in the square brackets. Since we neglect the selfenergy, the propagator $G(p) = [ip_0 + e(\mathbf{p})]^{-1} \chi_\Lambda(p)$ is the free propagator multiplied with an appropriate cutoff function. That is, although not denoted explicitly, it is understood throughout that the propagator $G(p)$ depends on scale Λ . This flow equation is derived in [25].

Since the initial vertex function U of the Hubbard model obeys the following symmetries, the flow equation implies that the effective vertex function V_Λ satisfies

$$\begin{aligned} V_\Lambda(p_1, p_2, p_3) &= V_\Lambda(p_3, p_1 + p_2 - p_3, p_1) & (\text{PHS}) \\ V_\Lambda(p_1, p_2, p_3) &= V_\Lambda(p_2, p_1, p_1 + p_2 - p_3) & (\text{RAS}). \end{aligned} \quad (5)$$

The first symmetry expresses invariance of the partition function as a functional integral under a change of integration variables $\psi \mapsto i\bar{\psi}$ and $\bar{\psi} \mapsto i\psi$ and is called particle hole symmetry (PHS). The second symmetry is directly inherited from (3) and accounts for remnants of the antisymmetry (RAS) of the Grassmann variables.

3 Decomposition of the Effective Interaction

The parametrization of the vertex function developed in this section is based on the observation that mainly the singular momentum structure of the RG equation determines the qualitative instabilities of the flow. That is, the parametrization of V should simplify the momentum dependence but should keep track of all possible singular contributions. If the vertex function is regular, the only momentum dependence that can change the singular behavior of the RG equation is the transfer momentum that propagates through the scale-derivative of the particle-particle or particle-hole bubble

$$\dot{\Phi}_{\text{pp/ph}}(l) = \frac{d}{d\Lambda} \int dp G(p) G(l \mp p). \quad (6)$$

In order to absorb this momentum dependence we introduce three additional channels corresponding to three different transfer momenta in the RG equation respectively

$$\mathcal{V}_\Lambda[\Psi] = \mathcal{V}_{\text{H.M.}}[\Psi] + \mathcal{V}_{\text{SC}}^\Lambda[\Psi] + \mathcal{V}_{\text{M}}^\Lambda[\Psi] + \mathcal{V}_{\text{K}}^\Lambda[\Psi]. \quad (7)$$

The initial on-site interaction of the Hubbard model $\mathcal{V}_{\text{H.M.}}[\Psi]$ is kept in the parametrization since there are ambiguities in assigning it to the other channels. It will remain constant in the flow and can be seen as a driving force. This does not mean that the on-site term contained in the full interaction (7) remains independent of scale.

The corrections to it are absorbed as contributions to the additional channels

$$\begin{aligned}
\mathcal{V}_{\text{SC}}^\Lambda[\Psi] &= -\frac{1}{4} \int dq dq' dl \Phi_{\text{SC}}^\Lambda(q, q', l) \sum_{J=0}^3 \left(\bar{\Psi}(q) \sigma^{(J)} \bar{\Psi}(l-q) \right) \left(\Psi(q') \sigma^{(J)} \Psi(l-q') \right) \\
\mathcal{V}_{\text{M}}^\Lambda[\Psi] &= -\frac{1}{4} \int dq dq' dl \Phi_{\text{M}}^\Lambda(q, q', l) \sum_{j=1}^3 \left(\bar{\Psi}(q) \sigma^{(j)} \Psi(q+l) \right) \left(\bar{\Psi}(q') \sigma^{(j)} \Psi(q'-l) \right) \\
\mathcal{V}_{\text{K}}^\Lambda[\Psi] &= -\frac{1}{4} \int dq dq' dl \Phi_{\text{K}}^\Lambda(q, q', l) \left(\bar{\Psi}(q) \Psi(q+l) \right) \left(\bar{\Psi}(q') \Psi(q'-l) \right), \tag{8}
\end{aligned}$$

where $\sigma^{(J)}$ are the Pauli matrices for $J = 1, 2, 3$ and $\sigma^{(0)}$ is the two-dimensional unit matrix. Each of the channels (8) is a general $U(1)$ and $SU(2)$ symmetric two-fermion interaction. We call them the superconducting, magnetic, and forward scattering channel respectively. These names are legitimate if the functions Φ_{SC} , Φ_{M} , and Φ_{K} are regular in their first two momentum indices and possibly singular only in the third (bosonic) momentum index l . Note that the Φ 's are zero at the beginning and are generated in the flow. In order to define their evolution we use the standard Fierz identity $\frac{1}{2} \sum_{J=0}^3 \sigma_{\sigma_1 \sigma_2}^{(J)} \sigma_{\sigma_3 \sigma_4}^{(J)} = \delta_{\sigma_1 \sigma_4} \delta_{\sigma_2 \sigma_3}$ to restate (8) in terms of a vertex function

$$\begin{aligned}
V_\Lambda(p_1, p_2, p_3) &= U - \Phi_{\text{SC}}^\Lambda(p_1, p_3, p_1 + p_2) + \Phi_{\text{M}}^\Lambda(p_1, p_2, p_3 - p_1) \\
&\quad + \frac{1}{2} \Phi_{\text{M}}^\Lambda(p_1, p_2, p_2 - p_3) - \frac{1}{2} \Phi_{\text{K}}^\Lambda(p_1, p_2, p_2 - p_3) \tag{9}
\end{aligned}$$

and insert it into the RG equation. The strong momentum dependence of the superconducting channel should be the sum of the two incoming particles $p_1 + p_2$ which is the transfer momentum of the particle-particle graph. Likewise the combinations $p_3 - p_1$ and $p_2 - p_3$ are the transfer momenta of the crossed and direct particle-hole graphs respectively. So we define

$$\begin{aligned}
\dot{\Phi}_{\text{SC}}^\Lambda(p_1, p_3, p_1 + p_2) &= -\mathcal{T}_{\text{pp}}(p_1, p_2, p_3) \\
\dot{\Phi}_{\text{M}}^\Lambda(p_1, p_2, p_3 - p_1) &= \mathcal{T}_{\text{ph}}^{\text{cr}}(p_1, p_2, p_3) \\
\dot{\Phi}_{\text{K}}^\Lambda(p_1, p_2, p_2 - p_3) &= -2\mathcal{T}_{\text{ph}}^{\text{d}}(p_1, p_2, p_3) + \mathcal{T}_{\text{ph}}^{\text{cr}}(p_1, p_2, p_1 + p_2 - p_3). \tag{10}
\end{aligned}$$

This decomposition of the interaction vertex into three channels is exact at one-loop level and the symmetries (PHS) and (RAS) are satisfied by each channel, that is

$$\begin{aligned}
\Phi_{\text{SC}}^\Lambda(q, q', l) &= \Phi_{\text{SC}}^\Lambda(l - q, l - q', l) = \Phi_{\text{SC}}^\Lambda(q', q, l) \\
\Phi_{\text{M/K}}^\Lambda(q, q', l) &= \Phi_{\text{M/K}}^\Lambda(q', q, -l) = \Phi_{\text{M/K}}^\Lambda(q + l, q' - l, -l). \tag{11}
\end{aligned}$$

The first identity in each line corresponds to (RAS) and can be directly seen from (8), whereas the second identity corresponds to (PHS). Both symmetries follow from the defining flow equations (10). Therefore (9) satisfies (RAS) and (PHS).

In summary, the definition of the channels is chosen such that each channel carries one critical momentum dependence. If the vertex function is still regular, all possible singular momentum dependence of the flow equation is absorbed by the channels. Furthermore, the decomposition satisfies (RAS) and (PHS). The assignment of the graphs, however, is not unique for special momenta. For example, a constant term can be freely distributed among the channels. Nevertheless, we have uniquely defined the channels assuming that the different classes of graphs with their corresponding transfer momenta form a natural decomposition. This is the only definition such that each channel absorbs one singular momentum and such that (if the transfer momentum becomes singular) the channels correspond to interactions of Cooper pairs, spin operators, and density operators respectively as written in (8).

Next we further decompose the interaction vertex by writing each channel as an interaction of two fermion bilinears interacting via an exchange boson. Naturally, the critical transfer momentum, which as a sum of two fermion momenta is a boson momentum, is chosen to be the momentum of the boson propagator. Due to (PHS), $\Phi_{\text{SC}}(q, q', l) = \Phi_{\text{SC}}(q', q, l)$ and we can expand

$$\Phi_{\text{SC}}^{\Lambda}(q, q', l) = \sum_{m, n \in \mathcal{I}_{\text{SC}}} D_{mn}(l) f_m(\frac{1}{2} - \mathbf{q}) f_n(\frac{1}{2} - \mathbf{q}') + R_{\text{SC}}(q, q', l), \quad (12)$$

such that $\mathcal{V}_{\text{SC}}[\Psi]$ describes the interaction of Cooper pairs via the boson propagator $D(l)$ up to a remainder term R_{SC} . Actually, Φ_{SC} as a function of its first two indices can be regarded as the kernel of a Fredholm operator. But since we are not able to determine the scale-dependent eigenfunctions, we expand in a given (scale-independent) finite set of form factors $(f_n)_{n \in \mathcal{I}_{\text{SC}}}$ and leave a remainder. The form factors are orthonormalized on full momentum space $(-\pi, \pi]^2$ (divided by $4\pi^2$) and depend only on the relative momentum of the Cooper pairs, representing different singlet and triplet lattice symmetries. In principle an expansion in momentum and frequency degrees of freedom is possible. For simplicity we take an approach where the form factors (in contrast to the boson propagator D) do not depend on frequency. This leaves an ambivalence in the definition of D such that the expansion (12) is satisfied. We set the frequency corresponding to q and q' to $\frac{l_0}{2}$, which is a fermion frequency since l_0 is a boson frequency. The leading instability will occur at $l_0 = 0$ so in that case $q_0 = q'_0 = 0$ which will give the main contribution. For $\beta < \infty$ this is an overestimate since the lowest possible (absolute) value of a fermion frequency is $\pm \frac{\pi}{\beta}$. Alternatively for finite temperature, q_0 and q'_0 could be set to $\frac{l_0}{2} \pm \frac{\pi}{\beta}$ and $\frac{l_0}{2} \mp \frac{\pi}{\beta}$ respectively, with symmetrization over the sign. That is, for $m, n \in \mathcal{I}_{\text{SC}}$, the coefficient $D_{mn}(l)$ in (12) is given by

$$D_{mn}(l) = \int \frac{d^2 \mathbf{q}}{(2\pi)^2} \frac{d^2 \mathbf{q}'}{(2\pi)^2} f_m(\frac{1}{2} - \mathbf{q}) f_n(\frac{1}{2} - \mathbf{q}') \Phi_{\text{SC}}(q, q', l) \Big|_{q_0=q'_0=\frac{l_0}{2}}. \quad (13)$$

With this choice of definition, (RAS) implies $D_{mn}(l) = D_{nm}(l) = \sigma_m \sigma_n D_{mn}(l)$ where $f_n(\mathbf{p}) = \sigma_n f_n(-\mathbf{p})$ with σ_n either $+$ or $-$. Therefore, D is a block matrix with separate blocks for singlet and triplet symmetry.

Likewise the magnetic and forward scattering channels are expanded. Now by (RAS), $\Phi_{\text{M/K}}(q, q', l) = \Phi_{\text{M/K}}(q', q, -l)$, so we can write

$$\begin{aligned}\Phi_{\text{M}}^{\Lambda}(q, q', l) &= \sum_{m, n \in \mathcal{I}_{\text{MK}}} M_{mn}(l) f_m(\mathbf{q} + \tfrac{1}{2}) f_n(\mathbf{q}' - \tfrac{1}{2}) + R_{\text{M}}(q, q', l) \\ \Phi_{\text{K}}^{\Lambda}(q, q', l) &= \sum_{m, n \in \mathcal{I}_{\text{MK}}} K_{mn}(l) f_m(\mathbf{q} + \tfrac{1}{2}) f_n(\mathbf{q}' - \tfrac{1}{2}) + R_{\text{K}}(q, q', l)\end{aligned}\quad (14)$$

with symmetric boson propagators $M_{mn}(l) = M_{nm}(-l)$ and $K_{mn}(l) = K_{nm}(-l)$ and remainder terms R_{M} and R_{K} . The functions $(f_n)_{n \in \mathcal{I}_{\text{MK}}}$ are again scale-independent, orthonormalized on $(-\pi, \pi]^2$, and frequency independent. Although different expansions for the magnetic and forward scattering channel are possible, we choose the same for notational simplicity. The index sets \mathcal{I}_{SC} and \mathcal{I}_{MK} need not be the same. In analogy to the superconducting boson propagator we set

$$\begin{aligned}M_{mn}(l) &= \int \frac{d^2 \mathbf{q}}{(2\pi)^2} \frac{d^2 \mathbf{q}'}{(2\pi)^2} f_m(\mathbf{q} + \tfrac{1}{2}) f_n(\mathbf{q}' - \tfrac{1}{2}) \Phi_{\text{M}}(q, q', l) \Big|_{q_0 = -\frac{l_0}{2}, q'_0 = \frac{l_0}{2}} \\ K_{mn}(l) &= \int \frac{d^2 \mathbf{q}}{(2\pi)^2} \frac{d^2 \mathbf{q}'}{(2\pi)^2} f_m(\mathbf{q} + \tfrac{1}{2}) f_n(\mathbf{q}' - \tfrac{1}{2}) \Phi_{\text{K}}(q, q', l) \Big|_{q_0 = -\frac{l_0}{2}, q'_0 = \frac{l_0}{2}}.\end{aligned}\quad (15)$$

With the boson propagators defined in this way the three expansions and the remainder terms fulfill (RAS) and (PHS) separately. The magnetic interaction describes interacting spin operators. For example, a constant $f_{\text{s}}(\mathbf{p}) = 1$ describes a local spin operator and a further expansion in the s -wave channel generalizes to nearest neighbors and next to nearest neighbors and so on. A d -wave form factor in the forward scattering expansion describes a possible Pomeranchuk instability [6].

So far we have decomposed the interaction vertex such that boson propagators carry the critical momentum dependence of the right hand side of the RG equation at least as long as the effective vertex function is regular. If it can be shown that the remainder terms R_{SC} , R_{M} , and R_{K} remain regular or at least less singular than the boson propagators (even if the effective vertex function develops a singularity in the flow), then several benefits are gained for the analysis of competing instabilities. First, the decomposition of the interaction allows to identify qualitatively which instabilities are favored. After the flow is stopped, the dominant terms in the interaction can be decoupled by Hubbard–Stratonovich transformations, so that one can proceed with a bosonic flow. Furthermore, the parametrization of the flow is simplified, since no function of three fermion momenta and frequencies has to be studied, but only several functions of one fermion momentum and frequency. The boson fields involved have point singularities, which pose substantially less numerical effort than the extended Fermi surface singularities.

4 The Superconducting Channel

In this section we consider an example to illustrate our method. Let the Fermi surface be curved and regular. By this we mean that the Fermi surface does not

meet the Van Hove points and that Umklapp scattering is irrelevant. Then the particle-hole bubble is negligible compared to the particle-particle bubble, which develops a strong peak for small momentum and frequency.

In a first step the particle-hole graphs are altogether neglected. The RG equation (4) without selfenergy effects is then solved by the solution of a self-consistency equation

$$V_\Lambda(q, l - q, q') = V_{\Lambda_0}(q, l - q, q') - \int dp G(p)G(l - p)V_{\Lambda_0}(q, l - q, p)V_\Lambda(l - p, p, q'), \quad (16)$$

where $G(p) = [ip_0 - e(\mathbf{p})]^{-1}\chi_\Lambda(p)$ is the free fermion propagator multiplied with a regulator function $\chi_\Lambda(p)$. In this section we choose a strict Fermi surface momentum cut-off, that is, modes with $|e(\mathbf{p})| < \Lambda$ are suppressed completely. If the vertex function is expanded in a complete set of Λ independent functions f_n but Λ dependent coefficients $\nu_{mn}^\Lambda(l)$

$$V_\Lambda(q, l - q, q') = V_\Lambda(q', l - q', q) = \sum_{m,n} \nu_{mn}^\Lambda(l) f_m(\frac{l}{2} - q) f_n(\frac{l}{2} - q'),$$

then the self-consistency equation (16) is solved by $\nu^\Lambda = A^{-1}$, where the scale-dependent matrix $A_{mn}(l) = (\nu^{\Lambda_0})_{mn}^{-1}(l) + \Phi_{pp}^{mn}(l)$ is given by the initial condition and the particle-particle bubble

$$\Phi_{pp}^{mn}(l) = \int dp G(p)G(l - p) f_m(\frac{l}{2} - p) f_n(\frac{l}{2} - p). \quad (17)$$

We concentrate on the singular case $l = 0$. If the functions f_n could be chosen such that $\Phi_{pp}^{mn}(0)$ and $(\nu^{\Lambda_0})_{mn}^{-1}(0)$ are both diagonal, then the matrix $A(0)$ could easily be inverted to give $\nu_{mn}^\Lambda(0) = \nu_n^{\Lambda_0}(0)[1 + \nu_n^{\Lambda_0}(0)\Phi_{pp}^{nn}(0)]^{-1}\delta_{mn}$. If there is an attractive channel in the initial condition, that is $\nu_n^{\Lambda_0} < 0$ for some n , the flow in this channel diverges for large enough β due to a zero in the denominator. On the other hand, the flow of ν_n^Λ is asymptotically free for all n with $\nu_n^{\Lambda_0} > 0$ (repelling).

However, $\Phi_{pp}^{mn}(0)$ is not diagonal in general. Suppose that the functions f_n do not depend on frequency. Following [28] we change variables $\mathbf{p} = \pi(E, \theta)$ with $E = e(\mathbf{p})$ and an angle θ to obtain

$$\Phi_{pp}^{mn}(0) = \int_{\Lambda}^{\Lambda_0} dE \frac{\tanh \frac{\beta E}{2}}{2E} \int d\theta J(E, \theta) f_m(\pi(E, \theta)) f_n(\pi(E, \theta))$$

with Jacobian $J(E, \theta)$. The θ -integral is a smooth function of E for a curved and regular Fermi surface. For Λ_0 small enough the zeroth order of a Taylor expansion in E , that is a projection onto the Fermi surface, gives diagonality if the f_n 's are chosen as Fermi surface harmonics [1]. Therefore the main contribution of $\Phi_{pp}^{mn}(0)$ can be made diagonal for a curved and regular Fermi surface.

This gives a good understanding of the flow in the superconducting channel (12). In a diagonal expansion of dominant processes only form factors that give rise to positive boson propagators have to be taken into account. All other terms in the expansion are suppressed to zero and can be neglected since they will not influence the qualitative behavior of the flow. In practice one suspects that only the biggest positive coefficient plays a role in the flow to strong coupling (depending on the size of the corresponding bubble).

For a non-diagonal expansion one cannot separate the irrelevant modes exactly. There will be a flow to strong coupling if $\det A = 0$ (for any finite expansion) at some scale. However, since diagonality holds approximately, there is a good chance to capture the singular behavior of A in a small matrix of well-chosen form factors.

In a second step we take into account the full one-loop RG equation with all particle-particle and particle-hole graphs and start with the initial repulsive Hubbard interaction. Due to the curved and regular Fermi surface and negligible Umklapp scattering assumed in this section, we only consider the superconducting channel and decompose

$$V_\Lambda(q, l - q, q') = - \sum_{m, n \in \mathcal{I}_{\text{SC}}} D_{mn}(l) f_m(\frac{1}{2} - \mathbf{q}) f_n(\frac{1}{2} - \mathbf{q}') + U + R(q, l - q, q'). \quad (18)$$

As discussed above we select only a few form factors that describe the superconducting channel correctly and drop the remainder term R_{SC} of the expansion in the superconducting channel (12).³ The function R in (18) arises from particle-hole graphs. We will study its influence on the flow in the superconducting channel and show that the Kohn-Luttinger effect is present in our method. That is, although starting at Λ_0 with a repelling $V_{\Lambda_0}(q, l - q, q') = U > 0$, particle-hole terms will create an attractive superconducting interaction.

Inserting the decomposition (18) into the RG equation (4) and projecting the particle-particle graphs according to (13) gives the flow equation for the superconducting boson propagators for $n, m \in \mathcal{I}_{\text{SC}}$

$$\begin{aligned} \dot{D}_{mn}(l) = \sigma_n \int d\mu(p, l - p) & \left[\sum_{a \in \mathcal{I}_{\text{SC}}} D_{ma}(l) f_a(\frac{1}{2} - \mathbf{p}) - \delta_{m,s} U - \alpha_m(p, l) \right] \\ & \times \left[\sum_{a' \in \mathcal{I}_{\text{SC}}} D_{na'}(l) f_{a'}(\frac{1}{2} - \mathbf{p}) - \delta_{n,s} U - \alpha_n(p, l) \right] \end{aligned} \quad (19)$$

with initial values $D_{mn}(l) = 0$ at scale Λ_0 and with the contribution from the particle-hole channels $\alpha_m(p, l) = \int \frac{d^2 \mathbf{q}}{(2\pi)^2} f_m(\frac{1}{2} - \mathbf{q}) R(q, l - q, p)|_{q_0=l_0/2}$. We denote $d\mu(p, k) = \frac{d}{d\Lambda} (G(p)G(k)) dp$ for the bubble integration and $f_m(-\mathbf{p}) = \sigma_m f(\mathbf{p})$ distinguishes between singlet and triplet symmetry. Further we assume that \mathcal{I}_{SC} contains the index $n = s$ where $f_s(\mathbf{p}) = 1$ is the constant form factor.

³In particular, since the form factors do not depend on frequency, we assume that the frequency dependence of the vertex function is described well by the singular frequency l_0 .

The evolution of R is given by the particle-hole graphs, which unlike the particle-particle graphs remain bounded at all scales. In the beginning of the flow D is still small, so we neglect all particle-hole graphs proportional to D . We further neglect the remaining direct particle-hole graphs since they cancel exactly for a constant vertex function, hence remain small for a nearly constant vertex function. (The initial condition is $V_{\Lambda_0} = U$, that is, constant.) Then the flow equation for R , given by crossed particle-hole graphs only, is solved by $R(q, l - q, q') = \psi(q' - q) - U$ with $\psi(l) = U[1 + U\Phi_{\text{ph}}(l)]^{-1}$ where $\Phi_{\text{ph}}(l) = \int dp G(p)G(p+l)$ is the particle-hole bubble.

Although $\Phi_{\text{ph}}(l) < 0$ (for $l_0 = 0$), the denominator of ψ remains nonzero for a sufficiently small initial coupling U since the particle-hole bubble is bounded in case of a curved and regular Fermi surface. So $\psi(l)$ is a regular (smooth for an appropriate cut-off) and symmetric function that can be expanded in the form factors we are interested in. Again, the frequency dependence of ψ is not taken into account here. Neglecting possible remainders of this expansion, the flow equation for the superconducting boson propagator reads

$$\dot{D}_{mn}(l) = \sigma_n \sum_{a,a' \in \mathcal{I}_{\text{SC}}} \left[D_{ma}(l) - b_{ma} \right] \dot{\Phi}_{\text{pp}}^{aa'}(l) \left[D_{a'n}(l) - b_{a'n} \right], \quad (20)$$

where $b_{aa'} = \int \frac{d^2\mathbf{q}}{(2\pi)^2} \frac{d^2\mathbf{q}'}{(2\pi)^2} \psi(q' - q) \big|_{q_0=q'_0} f_a(\mathbf{q}) f_{a'}(\mathbf{q}')$.

If we only take into account two form factors $\mathcal{I}_{\text{SC}} = \{s, 1\}$ with $f_s(\mathbf{p}) = 1$ (s -wave) and $f_1(\mathbf{p}) = \cos p_x - \cos p_y$ ($d_{x^2-y^2}$ -wave), then $b_{s1} = b_{1s} = 0$, so b is diagonal as is $\Phi_{\text{pp}}^{aa'}(0)$ in this case. Then the boson propagator $D_{mn}(0)$ is diagonal as well and the flow equation (20) factorizes for $l = 0$ such that the right hand side is always positive. The coefficient b_{ss} is of order U and positive, so D_{ss} is suppressed to zero. That is, s -wave superconductivity is always suppressed by the initial repulsive interaction. On the other hand b_{11} is of order U^2 and negative, so $D_{11}(0)$ grows without bounds. Therefore, particle-hole fluctuations induce an attractive d -wave pairing interaction, which will be essential for the study of superconductivity in the Hubbard model at Van Hove filling. Here we have not included triplet superconductivity, which can become dominant as well. In general, attractive interactions in the Cooper channel are induced, so our method does capture the Kohn-Luttinger effect. The approximations made are valid provided the scale is not too low.

In summary, the proposed decomposition of the interaction vertex is well understood for a curved and regular Fermi surface, where there is no Van Hove singularity and where Umklapp scattering is irrelevant. Namely, if the expansion in form factors is diagonal, we gave a clear argument which form factors have to be included in the expansion, such that the remainder of the expansion is negligible. In the general case diagonality holds approximately. The influence of subdominant particle-hole fluctuations can become important if there is no strong attractive interaction already initially.

However, if Umklapp scattering and a Van Hove singularity in the density of states are present, particle-hole fluctuations can diverge by themselves and the mix-

ing between particle–particle and particle–hole channels is strong. This case is not analytically understood yet and treated numerically in the following.

5 Ω –Scheme and Integration over High Scales

Although the renormalization group idea is independent of the type of regularization used to define the flow (provided the regularization satisfies some minimal conditions, e.g. that it makes the flow equation well–defined), its choice can become a delicate matter once approximations are used. In particular, we restrict the flow to the symmetric phase and apply the one–loop truncation. Parts of the vertex function will grow strongly at small scales, indicating an instability to an ordered (symmetry broken) state. Since we are using a weak coupling scheme, we have to stop the flow before all modes are integrated out, that is, the full model is not recovered in the flow. Therefore, the one–loop flow confined to the symmetric phase may depend on the type of regularization, and one has to compare the results of different regularization schemes.

Since we are especially interested in the interplay between d –wave superconductivity and ferromagnetism, we have to choose a regularization that does not suppress small momentum particle–hole fluctuations [12]. In the Hubbard model at Van Hove filling the density of states diverges logarithmically at low single–particle energies. At zero temperature and without scale regularization, the particle–hole bubble at zero momentum transfer is given by minus the density of states. Therefore, the particle–hole bubble at zero momentum transfer and zero temperature should diverge logarithmically at low energy scales in the presence of a Van Hove singularity. However, for example, this is not the case for a Fermi surface cut–off which, at all nonzero scales, suppresses the small–momentum particle–hole excitations completely (see the discussion in [12]). For such a Fermi surface cut–off the particle–hole bubble at zero momentum transfer is zero for all finite scales at temperature zero. Even for nonzero temperature this means an artificial suppression of small momentum particle–hole processes down to the very lowest scales. Instead of a Fermi surface cut–off we multiply the bare propagator with the regulator function

$$\chi_{\Omega}(p) = \frac{p_0^2}{p_0^2 + \Omega^2}, \quad (21)$$

which is independent of momentum but depends on frequency. The frequency Ω is the scale parameter we use to generate the RG flow and it replaces the Λ we used in the general discussion in Section 2. Since possible zeros of the denominator in the integrand of the bubble integration are canceled, the bubbles are regularized for all temperatures if the scale $\Omega > 0$. Small momentum particle–hole processes are not artificially suppressed to lowest scales with this regularization since the particle–hole bubble, now formed with the Ω –dependent propagator $G(p) = [ip_0 - e(\mathbf{p})]^{-1} \chi_{\Omega}(p)$, has the right asymptotic scaling behavior at temperature zero and Van Hove filling,

that is $\Phi_{\text{ph}}(0) \sim \log \Omega$. The particle–particle bubble $\Phi_{\text{pp}}(0) \sim (\log \Omega)^2$ diverges faster for the same parameters, as expected.

In the limit $\Omega \rightarrow \infty$ the regulator function (21) vanishes, hence the vertex function is the initial on–site interaction U of the Hubbard model. For $\Omega \rightarrow 0$, $\chi_{\Omega}(p) \rightarrow 1$, i.e. the regulator is removed. The regularization is mild, but it suffices to make all loop integrals in the flow equation converge. Thus it is an admissible scheme. For brevity we call this regularization the Ω –scheme.

Because perturbation theory converges for large Ω [21, 27], we fix a scale Ω_0 and perform the integration over the degrees of freedom with propagator $(1 - \chi_{\Omega_0}(p))[ip_0 - e(\mathbf{p})]^{-1}$ by perturbation theory. The result provides the initial condition for the flow at scale $\Omega = \Omega_0$. To second order in U this gives for the Hubbard model in terms of a vertex function as in equation (3),

$$V_{\Omega_0}(p_1, p_2, p_3) = U - U^2 \Phi_{\text{pp}}(p_1 + p_2) - U^2 \Phi_{\text{ph}}(p_3 - p_1) + \mathcal{O}(U/\Omega_0)^3, \quad (22)$$

where the first term is the initial Hubbard repulsion. The second term is the particle–particle bubble, which generates an attractive s –wave superconducting channel. It will always be dominated by the repulsion U . The third term in (22) comes from the crossed particle–hole graph. The contribution from the direct particle–hole graphs cancels out because the Hubbard interaction is on–site.

We choose the initial condition for the boson propagators at scale Ω_0 as

$$\begin{aligned} D_{\text{ss},0}(l) &= U^2 \Phi_{\text{pp}}(l) \\ M_{\text{ss},0}(l) &= K_{\text{ss},0}(l) = -U^2 \Phi_{\text{ph}}(l) > 0 \end{aligned} \quad (23)$$

for the constant s –wave form factor $f_s(\mathbf{p}) = 1$. The symmetric part of $D_{\text{ss},0}(l)$ is positive as well, as is $D_{\text{ss},0}(l_0 = 0, \mathbf{l})$. This assignment of the result of perturbation theory to the initial boson propagators is not unique. For example, attracting parts of the particle–hole term could be absorbed in a superconducting d –wave term. But the assignment (23) is consistent with the definition of the three channels in Section 3, which do not mix in second order. Furthermore, the Kohn–Luttinger effect is very small in perturbation theory. The attractive coefficient of $d_{x^2-y^2}$ –superconductivity in an expansion of $U^2 \Phi_{\text{ph}}(p_3 - p_1)$ is bounded by $\sim 0.01 U^2$ even for low scales and remains finite if the scale regularization is removed. Therefore the ambiguity of (23) will not be important. In fact, we have numerically checked different distributions of the interaction terms in the initial conditions. We choose $\Omega_0 > U$ big enough such that the results presented in Section 8 do not depend on the initial conditions for the boson propagators. The latter are negligible compared to interactions generated in the flow by the local repulsion term linear in U . So for large enough Ω_0 our results are independent of the particular choice of Ω_0 .

6 RG Equations of the Boson Propagator Flow

In order to derive the RG equations for the boson propagators we insert the expansion of the three channels (12) and (14) into the RG equation (4) and project

the right hand side of it according to the definitions of the boson propagators (13) and (15). Similarly, equations for the remainder terms R_{SC} , R_{M} , and R_{K} can be obtained.

In case of a curved and regular Fermi surface we discussed in Section 4 how to separate singular from regular parts in the superconducting channel if the other channels are neglected. That gave a condition which form factors should be included in the expansion of the superconducting channel. Furthermore, as also analyzed in Section 4, we developed a good understanding of the integration of all one-loop graphs down to intermediate scales in this case. Therefore we argue that, with the right choice of form factors, the remainder terms can be dropped because the channels are described well even by only a few boson propagators.

In presence of Van Hove singularities and relevant Umklapp scattering, however, the mixing of the channels is very hard to control. Here we rely on the results of [6, 7, 13, 15, 33] and choose a combination of form factors corresponding to the main instabilities found there. A detailed study of the remainder terms is left for future work.

The flow equations derived in this section are valid for arbitrary index sets \mathcal{I}_{SC} and \mathcal{I}_{MK} , assuming they both contain the index s that stands for the constant form factor $f_s(\mathbf{p}) = 1$. If the remainder terms are dropped, then the flow equation for the superconducting boson propagator reads for $n, m \in \mathcal{I}_{\text{SC}}$

$$\begin{aligned} \dot{D}_{mn}(l) = \sigma_m \int d\mu(p, l-p) & \left[\sum_{a \in \mathcal{I}_{\text{SC}}} D_{ma}(l) f_a\left(\frac{1}{2} - \mathbf{p}\right) - U\delta_{ms} - \alpha_m^{\text{SC}}(p, l) \right] \\ & \times \left[\sum_{a \in \mathcal{I}_{\text{SC}}} D_{an}(l) f_a\left(\frac{1}{2} - \mathbf{p}\right) - U\delta_{ns} - \alpha_n^{\text{SC}}(p, l) \right], \end{aligned} \quad (24)$$

where $d\mu(p, l \pm p) = dp \frac{d}{d\Omega} G(p) G(l \pm p)$ is the bubble integration. The initial local repulsion U will suppress s -wave superconductivity D_{SS} . The contribution of the magnetic and forward scattering channels is given by

$$\begin{aligned} \alpha_m^{\text{SC}}(p, l) = \frac{1}{2} \int \frac{d^2 \mathbf{q}}{(2\pi)^2} f_m\left(\frac{1}{2} - \mathbf{q}\right) & \sum_{b, b' \in \mathcal{I}_{\text{MK}}} f_b\left(\frac{\mathbf{p} + \mathbf{q}}{2}\right) f_{b'}\left(\mathbf{1} - \frac{\mathbf{p} + \mathbf{q}}{2}\right) \\ & \times \left[(2 + \sigma_m) M_{bb'}(p - q) - \sigma_m K_{bb'}(p - q) \right] \Big|_{q_0 = \frac{l_0}{2}}. \end{aligned}$$

For example, the magnetic boson propagator M_{SS} induces an attracting interaction for $d_{x^2-y^2}$ -wave superconductivity as described in Section 4. The corresponding diagrams of the flow equation (24) are plotted in Figure 1 for singlet symmetry $\sigma_m = +1$ in a symbolic way. The graphs in the brackets are the superconducting, initial Hubbard repulsion, magnetic, and forward scattering interaction respectively. The square on the right hand side means that any two of the graphs in the bracket are put beside one another and connected to form one-loop diagrams. This generates three types of graphs, namely direct, vertex correction, and box graphs (see Figure

2). The latter two are not of the form of a boson propagator mediating between two fermion bilinears. We expand them in a sum of terms of that form (given by our ansatz for the interaction) and drop the remainder term. To get the coefficients in the expansion (12), we apply the projections equation.

$$\text{Diagram with circles m and n} = P_{mn}^{\text{SC}} \left[\text{Diagram with circles} - \text{Diagram with horizontal lines} - \frac{3}{2} \text{Diagram with triangles} + \frac{1}{2} \text{Diagram with squares} \right]^2$$

Figure 1: The graphical representation of the flow in the singlet superconducting channel.

In order to illustrate how the square in Figure 1 is applied, we state two examples. Taking two superconducting interactions and connecting them with two fermion propagators such that they form a loop, gives the direct graph in Figure 2(a). If the loop integration is performed, it is again of the form of two Cooper pairs interacting via a boson. By connecting a superconducting interaction with a magnetic interaction a vertex correction graph arises, given in Figure 2(b). This is not of the demanded form, so the projection is nontrivial. A box diagram, for example, is formed by connecting two magnetic interactions, see Figure 2(c).

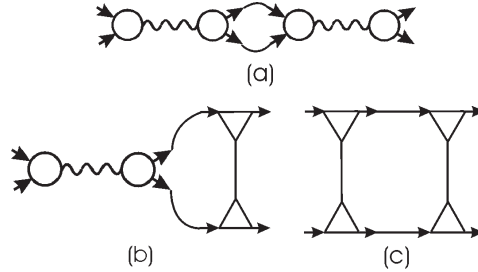


Figure 2: Three examples of arising graphs if the square in Figure 1 is taken: (a) the direct graph, (b) a vertex correction graph, and (c) a box graph.

In the magnetic channel the flow is described by

$$\dot{M}_{mn}(l) = - \int d\mu(p, p+l) \left[\sum_{b \in \mathcal{I}_{\text{MK}}} M_{mb}(l) f_b(\mathbf{p} + \frac{1}{2}) + U\delta_{ms} + \alpha_m^{\text{M}}(p, l) \right] \times \left[\sum_{b \in \mathcal{I}_{\text{MK}}} M_{bn}(l) f_b(\mathbf{p} + \frac{1}{2}) + U\delta_{ns} + \alpha_n^{\text{M}}(p, l) \right], \quad (25)$$

where

$$\alpha_m^M(p, l) = \frac{1}{2} \int \frac{d^2 \mathbf{q}}{(2\pi)^2} f_m(\mathbf{q} + \frac{1}{2}) \left[-2\sigma_m \sum_{a, a' \in \mathcal{I}_{SC}} D_{aa'}(p - q) f_a(\frac{\mathbf{p} + \mathbf{q}}{2} + \mathbf{l}) f_{a'}(\frac{\mathbf{p} + \mathbf{q}}{2}) \right. \\ \left. + \sum_{b, b' \in \mathcal{I}_{MK}} f_b(\frac{\mathbf{p} + \mathbf{q}}{2}) f_{b'}(\mathbf{l} + \frac{\mathbf{p} + \mathbf{q}}{2}) [M_{bb'}(p - q) - K_{bb'}(p - q)] \right] \Big|_{q_0 = -\frac{l_0}{2}}.$$

Again the initial Hubbard interaction contributes only to the local s -wave coupling part. It will drive the boson propagator M_{SS} . In contrast to that, the superconducting s -wave boson propagator D_{SS} will screen the local magnetic interaction M_{SS} . Because this effect is quite substantial, especially if U is not very small, D_{SS} is important and must be included in the flow, even though it does not become singular. The influence of $d_{x^2-y^2}$ superconductivity with form factor $f_1(\mathbf{p}) = \cos p_x - \cos p_y$ depends strongly on the boson momentum \mathbf{l} . It will suppress $M_{SS}(l)$ near $\mathbf{l} = 0$, that is, suppress ferromagnetism, and enhance $M_{SS}(l)$ near $\mathbf{l} = \hat{\pi} = (\pi, \pi)$, that is, antiferromagnetism, since $f_1(\mathbf{p} + \hat{\pi}) = -f_1(\mathbf{p})$. The symbolic representation with graphs of the flow equation (25) is given in Figure 3.

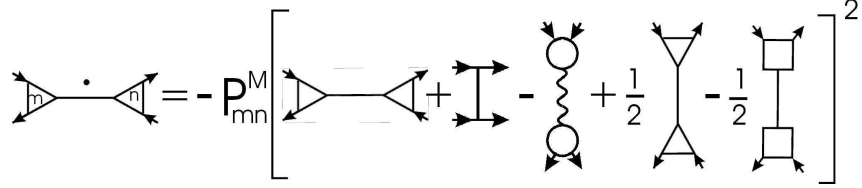


Figure 3: The flow in the magnetic channel.

Finally the flow equation for the forward scattering channel is given by

$$\dot{K}_{mn}(l) = - \int d\mu(p, p + l) \left[\sum_{b \in \mathcal{I}_{MK}} K_{mb}(l) f_b(\mathbf{p} + \frac{1}{2}) - U \delta_{ms} - \alpha_m^K(p, l) \right] \quad (26) \\ \times \left[\sum_{b \in \mathcal{I}_{MK}} K_{bn}(l) f_b(\mathbf{p} + \frac{1}{2}) - U \delta_{ms} - \alpha_n^K(p, l) \right]$$

with

$$\alpha_m^K(p, l) = \frac{1}{2} \int \frac{d^2 \mathbf{q}}{(2\pi)^2} f_m(\mathbf{q} + \frac{1}{2}) \left[2\sigma_m \sum_{a, a' \in \mathcal{I}_{SC}} (1 - 2\sigma_a) D_{aa'}(p - q) f_a(\frac{\mathbf{p} + \mathbf{q}}{2}) \right. \\ \left. \times f_{a'}(\mathbf{l} + \frac{\mathbf{p} + \mathbf{q}}{2}) \right. \\ \left. + \sum_{b, b' \in \mathcal{I}_{MK}} f_b(\frac{\mathbf{p} + \mathbf{q}}{2}) f_{b'}(\mathbf{l} + \frac{\mathbf{p} + \mathbf{q}}{2}) [3M_{bb'}(p - q) + K_{bb'}(p - q)] \right] \Big|_{q_0 = -\frac{l_0}{2}}.$$

Similarly to s -wave superconductivity K_{ss} is suppressed by U . In analogy to the Kohn–Luttinger effect a Pomeranchuk boson propagator K_{11} is induced by magnetic correlations. Graphically the equation is sketched in Figure 4.

Figure 4: The flow in the forward scattering channel.

We finish this section with some remarks on the just derived RG equations.

1. Instead of the Hubbard model consider a mean-field model. So set $U = 0$ and let the initial condition for the boson propagators be given by $D_{mn,0}(l) = D_{mn}^0 \delta_{l,0}$ and similarly for M and K . Then the flow equations recover mean-field theory in the thermodynamic limit. Only the direct graphs contribute in the thermodynamic limit since the α 's acquire an additional $\frac{1}{\beta L^2}$ factor.

2. Observing the flow equations, we find that the diagonal parts of the boson propagators at frequency zero are monotonically increasing. This is no contradiction to previous N -patch schemes where the measured susceptibilities did not need to be monotone. For example, the one-particle irreducible part of the connected expectation value

$$- \left\langle \int dp f_m(\frac{1}{2} - \mathbf{p}) \bar{\psi}(q) \frac{\epsilon}{2} \bar{\psi}(l - q); \int dp f_n(\frac{1}{2} - \mathbf{p}) \psi(q) \frac{\epsilon}{2} \psi(l - q) \right\rangle ,$$

which corresponds to the singlet superconducting susceptibility with $f_n(p) = f_n(-p)$, is here given by $D_{mn}(l)$ plus a contribution from the other channels. If the latter prevail, the slope of the subdominant susceptibility can change sign even for $n = m$ and $l = 0$.

3. The flow equations stated so far are quite general. They are valid for arbitrary sets of form factors \mathcal{I}_{SC} and \mathcal{I}_{MK} . Also, no assumptions have been made concerning the frequency and momentum dependence of the boson propagators. For a numerical solution we specify this momentum dependence in the next section. For given \mathcal{I}_{SC} and \mathcal{I}_{MK} this leads to substantial simplifications.

7 Momentum Dependence of the Boson Propagators

While we have chosen particular functions for the form factors, the frequency and momentum dependence of the boson propagators is not specified yet. If this dependence is not constrained, the RG equation for the boson propagators still remains a system of integro differential equations which is hard to solve. For the following numerical calculation we neglect the frequency dependence of the boson propagators.

Together with the frequency independent form factors, this corresponds to a vertex function that does not depend on frequency at all. The right hand side of the flow equations is evaluated at zero boson frequency, which gives the main contribution.

Furthermore we approximate the boson propagators by two-dimensional step functions. That is, their momentum dependence is discretized by dividing momentum space into segments on which the boson propagators are constant. Then the RG equation is equivalent to a system of x ordinary differential equations where x is the number of boson propagators times the number of segments. Note that the segments chosen here are neighborhoods of a single point because the boson propagators have point singularities. So they are different from the patches around the Fermi surface used in N -patch studies.

Thus the computational effort is reduced compared to Fermi surface N -patch schemes, where the frequency dependence is also neglected and $x \sim N^3$ with N the number of patches for one fermion momentum. In many N -patch studies N is reduced by projecting the momentum dependence onto the Fermi surface. This is not done here, we allow a general discrete momentum dependence of the boson propagators. It will turn out in the RG flow that the singular momentum dependence of the boson propagators is mainly determined by the fermion one-loop bubbles. Therefore, contrary to N -patch schemes, we can choose the size and alignment of the segments to gain a more accurate approximation by step functions.

For small scales and low temperature the bubbles can develop strong peaks at transfer momentum $\mathbf{l} = 0$ and $\mathbf{l} = \hat{\pi} = (\pi, \pi)$ (or at $\mathbf{l} = \hat{\pi} - \delta$ for incommensurate Umklapp scattering). Possible singularities of the boson propagators are closely related to the corresponding direct graphs, which have the same momentum dependence as the bubbles. Therefore we separate the momentum dependence of the boson propagators into two parts

$$B(\mathbf{l}) = B^{(0)}(\mathbf{l}) \mathbb{1}(|l_x| + |l_y| \leq \pi) + B^{(\hat{\pi})}(\mathbf{l} - \hat{\pi}) \mathbb{1}(|l_x - \pi| + |l_y - \pi| \leq \pi) \quad (27)$$

for $B = D, M$, or K representing the different boson propagators and $l_x, l_y \in [0, 2\pi)$ and periodically continued elsewhere. We now approximate $B^{(a)}(\mathbf{l})$, where $a = 0$ or $\hat{\pi}$, by step functions for $|l_x| + |l_y| \leq \pi$ with $l_x, l_y \in (-\pi, \pi]$. Singularities will appear for small $\mathbf{l} = (l_x, l_y)$ only. However, since we do not choose $U \ll 1$, the magnetic local propagators $M_{\text{ss}}^{(a)}(\mathbf{l})$ driven by U are not negligible for \mathbf{l} away from zero. Likewise, the propagators $D_{\text{ss}}^{(a)}(\mathbf{l})$ and $K_{\text{ss}}^{(a)}(\mathbf{l})$ are of order U for all momenta. Therefore the step functions have to cover full momentum space and not just a small neighbourhood of $\mathbf{l} = 0$.

Symmetries of the boson propagators can be used to reduce the number of step functions necessary. If the boson propagators are diagonal, then they obey the symmetries $B^{(a)}(l_x, l_y) = B^{(a)}(-l_x, -l_y) = B^{(a)}(l_y, l_x)$ where $a = 0$ or $\hat{\pi}$. In fact, for these symmetries to hold, the boson propagators are allowed to consist of block matrices for special form factors, such as f_1 and f_3 . Changing to polar variables $l_x = \rho \cos \phi$ and $l_y = \rho \sin \phi$, we divide the radial coordinate $\rho \in [0, \frac{\pi}{\sqrt{2}}]$ into n intervals as can be seen in Figure 5. We choose smaller segments for small ρ , that is,

for $k = 1, \dots, n$ the segments are $\left[\left(\frac{k-1}{n} \right)^\alpha \frac{\pi}{\sqrt{2}}, \left(\frac{k}{n} \right)^\alpha \frac{\pi}{\sqrt{2}} \right]$, where $\alpha \geq 1$ is a parameter for choosing the radial size of the smallest segment. The boson propagators are evaluated at the left border of each interval. Using the symmetries stated above, the angular variable ϕ needs only be discretized in $[-\frac{\pi}{4}, \frac{\pi}{4}]$. This range is divided into m homogeneous intervals, where the boson propagators are evaluated at the midpoints. The $k = 1$ radial segment has no angular dependence imposed. Since we want to cover $|l_x| + |l_y| \leq \pi$, one extra segment is needed for the difference of the disk to the square. This more inaccurate approximation for large momenta is justified since the singularity of the bubbles develops at small momenta near 0 or $\hat{\pi}$.

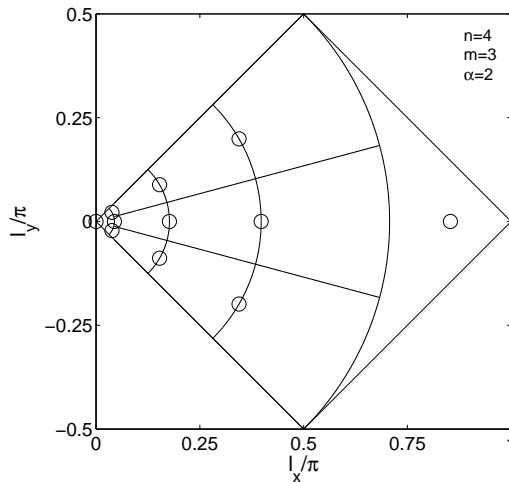


Figure 5: Schematic plot of the segment sizes for $n = 4$, $m = 3$, and $\alpha = 2$. The circles mark the spots where the boson propagators are evaluated. The momentum dependence of the boson propagators on full momentum space is obtained by using symmetries.

In the numerical calculation presented in the next section, we find that the magnetic and forward scattering boson propagators have sizeable contributions on a larger radial momentum range than the superconducting boson propagators, which have a strong peak for very small momenta only. This can also be observed in a comparison of the particle-particle and the particle-hole bubbles. Therefore we allow different α 's for these two cases.

Omitting the frequency dependence and parameterizing the momentum dependence with step functions simplifies the flow equations drastically for given form factors. The Matsubara frequency sum over the loop frequency p_0 can then be calculated explicitly. Also, by trigonometric identities the \mathbf{q} -integrations in the projections in α_m^{SC} , α_m^{M} , and α_m^{K} become sums of terms, whose dependence on the loop momentum \mathbf{p} can be stated analytically. Thus only the momentum loop integral has to be performed numerically to compute the flow.

8 Numerical Results at Van Hove Filling

We have numerically solved the flow equations for the boson propagators with different sets of form factors. Already a flow with only a constant form factor $f_s(\mathbf{p}) = 1$ in all channels plus standard $d_{x^2-y^2}$ -superconductivity with form factor $f_1(\mathbf{p}) = \cos p_x - \cos p_y$ in the superconducting channel gives reasonable results. We have checked that including the higher $d_{x^2-y^2}$ harmonic $f_3(\mathbf{p}) = \cos 3p_x - \cos 3p_y$ in the superconducting expansion produces only very small changes. Here we present results that are obtained by expanding all channels in the same set of form factors $\mathcal{I}_{\text{SC}} = \mathcal{I}_{\text{MK}} = \{s, 1\}$. Since $\Phi_{\text{pp}}^{\text{1s}}(a) = \Phi_{\text{ph}}^{\text{1s}}(a) = 0$ for $a = 0$ or $\hat{\pi}$, the boson propagators are diagonal at momentum $\mathbf{l} = 0$ or $\hat{\pi}$. Furthermore they are diagonal for all $|l_x| = |l_y|$ and this does not change in the flow. However, away from $|l_x| = |l_y|$ off-diagonal terms appear, which at first are neglected here since the singular structure of the boson propagators lies on these lines. At the end of this section we present results where off-diagonal boson propagators are included.

The density is set to Van Hove filling, that is, when varying the next to nearest neighbor hopping $-t'$ the particle number is changed to fit $\mu = 4t'$. With this choice of parameters the Hubbard model at weak coupling has a strong tendency towards ferromagnetism. Since we want to compare our results with those of the temperature RG flow [12], where ferromagnetism was first found in a one-loop RG method for the Hubbard model, we choose $U = 3$ as well.⁴ Smaller couplings are harder to treat numerically.

While in principle our method can treat all temperatures, for simplicity we here concentrate on temperature zero, which is not accessible within the temperature RG flow. However, starting at $\Omega_0 = 15$, we find that for all choices of t' , at least one of the boson propagators becomes almost singular at a point. In an approximation $(\mathbf{p}^2 + m_B^2)^{-1}$ for the boson propagator, one would say that the mass m_B of the boson tends to zero. However, the propagators are not well-approximated by this simple form, except maybe at very small momentum (depending on the scale Ω), and this is the main reason why we use a numerical method to capture the momentum dependence. The flow to strong coupling observed in previous fermionic RG studies is related to this pointlike singularity, in that certain approximations correspond to setting $p = 0$, which hides the fact that the interaction only becomes strong at points.

Although in our study, there is no flow to strong coupling in that sense, a true singularity in the interaction function introduces a significant change in power counting, which seems best to be captured by stopping the fermionic flow at a certain scale Ω_C , performing a transformation to exchange bosons, and then attempting to continue to the symmetry-broken phase. In our present study, we only consider the flow to the scale Ω_C , which we call the critical scale, and leave the other steps to future work. We stop the flow before the maximum of any boson propagator reaches $B_{\text{max}} = 20$. The thus defined critical scale, which roughly corresponds to a critical

⁴As noted before, all quantities are measured in units of $t = 1$.

temperature in the temperature flow, is plotted in Figure 6 over different hopping $-t'$. The flow to strong coupling of a boson propagator is interpreted as an instability to a corresponding ordered state. However, this can only give a qualitative picture of the actual ground state phase diagram. For the latter the flow has to be continued in the symmetry broken phase. So for example, the specific choice of B_{\max} is arbitrary. However, it does not effect the qualitative features of Figure 6. For $B_{\max} = 16$, for example, the critical scale is at most about 15% higher in the magnetic regions and even less in the superconducting region. Also, the range of $-t'$ where superconductivity dominates shrinks by less than 1%.

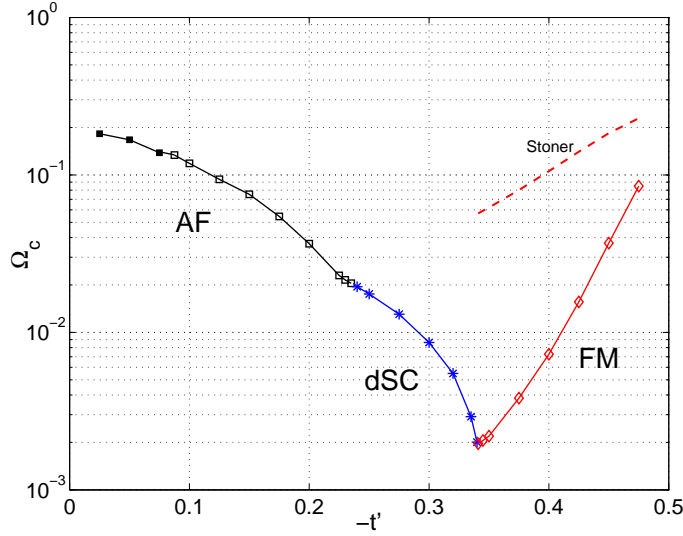


Figure 6: The critical scale in dependence on hopping $-t'$ at temperature zero and Van Hove filling for initial coupling $U = 3$. The instabilities of the Landau Fermi liquid are determined as antiferromagnetism (AF), $d_{x^2-y^2}$ superconductivity (dSC), and ferromagnetism (FM). The figure is further explained in the text.

As described in Section 7 we approximate the momentum dependence of the boson propagators by step functions, which are constant on segments in momentum space. Even for huge segments with $m = 1$ and $n = 4$ qualitatively consistent results are obtained, although the crossover values of $-t'$ between different instabilities as well as the critical scale are shifted compared to Figure 6, where we have used $m = 5$ and $n = 14$. For small and big $-t'$ the critical scale shows little dependence on different segment sizes, especially on the angular resolution. However, in the crossover region between superconductivity and ferromagnetism for intermediate $-t'$ the angular dependence becomes important, although the qualitative features of Figure 6 remain unchanged. Plotting the momentum dependence obtained in the flow, it can be seen that only the boson propagators $B^{(\hat{\pi})}$ away from small $-t'$ have a significant angular dependence. Those boson propagators have four identical maxima that move away from $\mathbf{l} = 0$ as $-t'$ is increased. In an angular sector that contains a max-

imum, they slowly increase on a high plateau for small increasing radial momentum. For higher radial momenta in the same sector they fall off rapidly after they passed the maximum, see also Figure 11(a) at the end of this section. On the other hand, in between angular sectors that contain a maximum, there are sectors where the value of the boson propagator decreases from $\mathbf{l} = 0$ on with increasing radial momenta. Consider for example Figure 7(a), where the antiferromagnetic boson propagator $M_{\text{ss}}^{(\hat{\pi})}$ is plotted at scale Ω_{C} and parameter $-t' = 0.3$. At this hopping the symmetric state is unstable towards $d_{x^2-y^2}$ superconductivity, which is induced by the antiferromagnetic boson propagator. Neglecting the angular momentum dependence of $M_{\text{ss}}^{(\hat{\pi})}$ results in a slightly higher Ω_{C} for superconductivity.

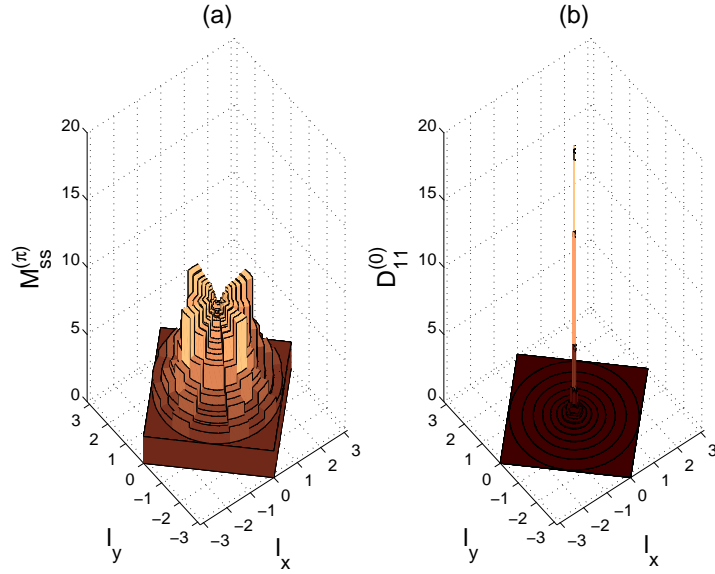


Figure 7: Momentum dependence of the boson propagators (a) $M_{\text{ss}}^{(\hat{\pi})}$ (antiferromagnetism) and (b) $D_{11}^{(0)}$ ($d_{x^2-y^2}$ superconductivity) at hopping $-t' = 0.3$ and critical scale Ω_{C} . The dependence is obtained by an approximation with step functions characterized by $m = 5$, $n = 14$, and $\alpha = 2$ in (a), and $\alpha = 3$ in (b). Although the peak in (b) is very sharp, the small segments chosen at small momenta describe it by more than one constant.

Generally, the magnetic and forward scattering boson propagators have sizeable contributions for a wide range of radial momenta, while the superconducting boson propagator D_{11} has a very strong peak at $\mathbf{l} = 0$, especially in the region where superconductivity is dominant. This can be seen in Figure 7(b) where D_{11} is plotted at Ω_{C} and hopping $-t' = 0.3$. In order to adapt to these different momentum scales we have chosen $\alpha_{\text{SC}} = 3$ for all superconducting boson propagators and $\alpha_{\text{MK}} = 2$ for all magnetic and forward scattering boson propagators.

Now we discuss Figure 6. For small $-t'$ the boson propagator $M_{\text{ss}}^{(\hat{\pi})}(\mathbf{l})$ at $\mathbf{l} = 0$

grows strongest, indicating an instability towards an antiferromagnetic phase. Since the flow is stopped at a relatively high scale $\Omega_C \sim 0.1$, perfect nesting-like effects are not restricted to $-t' = 0$. If $-t'$ is increased between $0.08 < -t' < 0.23$ the antiferromagnetic boson propagator is still the leading term. However its maximum is away from $\mathbf{l} = 0$, that is, it has four identical maxima, similar to Figure 7(a). This reflects a tendency to incommensurate antiferromagnetic order, indicated by open squares in Figure 6.

For $-t' \in [0.23, 0.34]$ the leading term is the superconducting boson propagator $D_{11}^{(0)}(\mathbf{l})$ at $\mathbf{l} = 0$, which represents $d_{x^2-y^2}$ -wave superconductivity. As discussed in Section 4, it is induced by antiferromagnetic correlations. In Figure 8(a) the flow of $D_{11}^{(0)}(0)$ is plotted for $-t' = 0.3$ in dependence on the scale. First incommensurate antiferromagnetic correlations dominate and $D_{11}^{(0)}(0)$ is enhanced by them but stays small down to low scales. When a significant superconducting coupling is reached, the direct graph $\sim D_{11}^{(0)}(0)^2 \dot{\Phi}_{\text{pp}}^{11}(0)$ contributes strongly such that $D_{11}^{(0)}(0)$ increases very fast and becomes the dominant coupling. The crossover between the antiferromagnetic and the $d_{x^2-y^2}$ superconducting region is not sharp in the scheme applied here. Around $-t' = 0.23$ both tendencies grow very strongly, making it difficult to judge numerically which is the dominant instability. The overlap of the two regions in Figure 9(a) corresponds to the saddle point region found earlier in [15].

As $-t'$ is increased the antiferromagnetic correlation, indicated by $|\Phi_{\text{ph}}(\hat{\pi})|$, decreases, while ferromagnetism is enhanced because $|\Phi_{\text{ph}}(0)|$ becomes bigger. Both affect the critical scale in the superconducting region, which is continuously dropping, especially when $-t'$ gets close to the ferromagnetic region. This indicates that $d_{x^2-y^2}$ superconductivity is not only induced by antiferromagnetic correlations but also suppressed by ferromagnetic tendencies.

For high $-t' > 0.34$ the leading instability is ferromagnetism, represented by the dominant flow of $M_{\text{ss}}^{(0)}(\mathbf{l} = 0)$. The critical scale rises again as $-t'$ increases. However, the critical scale is still about one order of magnitude lower than the Stoner criterion suggests. The Stoner criterion for ferromagnetism is obtained by neglecting the particle-particle channel and given by $U|\Phi_{\text{ph}}(0)| = 1$. Therefore superconducting fluctuations suppress ferromagnetism as well. However, outside the d -wave superconductivity region the superconducting d -wave boson propagator $D_{11}^{(0)}(\mathbf{l})$ remains small, see Figure 9(a) for its maximum at $\mathbf{l} = 0$. A significant contribution to this suppression comes from s -wave superconductivity $D_{\text{ss}}^{(0)}$ and $D_{\text{ss}}^{(\hat{\pi})}$, so-called screening, compare Figure 10.

In summary, ferromagnetism and d -wave superconductivity are competing instabilities of the (t, t') -Hubbard model for relatively large $-t'$ at Van Hove filling. In the calculation presented here the crossover between superconductivity and ferromagnetism takes place at $-t' = 0.34$ which is in good agreement with $-t' = 0.33$ found with the temperature RG flow [12] and the two-particle self-consistent Monte Carlo approach [8]. This is also roughly the value of $-t'$ where $\Phi_{\text{ph}}(0) = \Phi_{\text{ph}}(\hat{\pi})$. However, compared to the temperature RG flow, the suppression between these competing

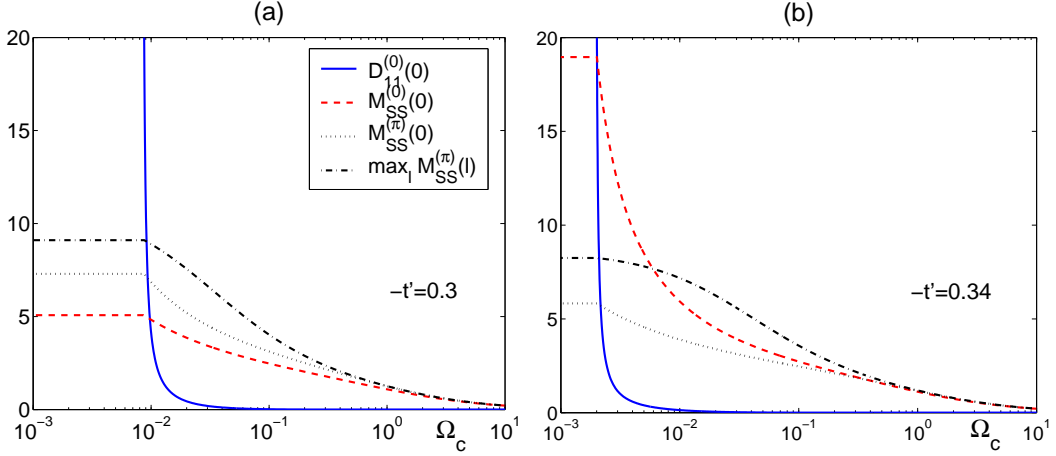


Figure 8: The dominant flows for two different values of $-t'$ in the superconducting region. The peak of the boson propagator $D_{11}^{(0)}$ at momentum zero evolves slowly but reaches the value 20 first. According to the definition of the critical scale Ω_c , the flow is stopped and all boson propagators are manually put constant for scales below Ω_c . In (a) $-t' = 0.3$ is well inside the superconducting region while in (b) $-t' = 0.34$ is the crossover to the ferromagnetic region. Here both instabilities grow strongly. Their mutual suppression results in a lower critical scale. In both figures antiferromagnetic fluctuations are dominant for intermediate scales, inducing $d_{x^2-y^2}$ superconductivity.

tendencies is weaker in the approximation used here. Although for low and high $-t'$ the critical scale Ω_c and the critical temperature from [12] is roughly the same, the temperature RG flow finds critical scales that are two orders of magnitude lower in the crossover region between superconductivity and ferromagnetism. Especially, the results obtained here do not suggest a quantum critical point separating these two instabilities in the phase diagram. Instead, in the crossover region both processes grow strongly like in the crossover between antiferromagnetism and superconductivity. However, the crossover is much sharper as can be seen in Figure 9(a). The superconducting boson propagator $D_{11}^{(0)}$ remains small as soon as $-t'$ enters the ferromagnetic region, while in the antiferromagnetic region superconducting tendencies persist, such that this crossover region is broader.

At present, it is not clear to us where this difference to [12] comes from, as both schemes contain rather different approximations. The RG equations for the boson propagators imply that their diagonal parts are monotonically increasing in the flow. Already a small inexactness, such as the omission of the remainder terms or the discretization of the momentum dependence, can prevent an exact cancellation on the right hand side of the flow equation for $D_{11}^{(0)}$ and $M_{SS}^{(0)}$. On the other hand, the projection to the Fermi surface, used in [12] but not here, is expected to enhance superconducting tendencies. This could possibly lead to a stronger sup-

pression. Furthermore, the Ω -scheme used here allows a clearer definition of the initial conditions than the temperature scheme. It would be interesting to perform an N -patch analysis with the proposed Ω -regularization (21).

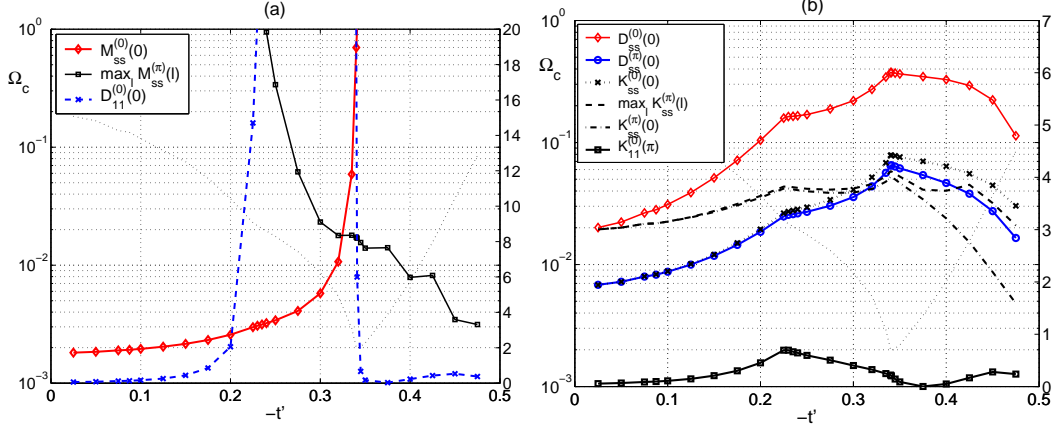


Figure 9: Overview of the maximal value of the boson propagators at the critical scale, which is plotted as a thin dotted line. In (a) the three dominant instabilities are plotted, that is antiferromagnetism, $d_{x^2-y^2}$ superconductivity, and ferromagnetism. The maxima of some subleading boson propagators are plotted in (b). The kinks in the plot indicate the crossovers to another dominant instability. For large $-t'$ the discretization scheme for the momentum dependence becomes insufficient for the antiferromagnetic boson propagator, whose four maxima move towards the edge of its support. Due to the large segment sizes there, $\max_l M_{ss}^{(\hat{\pi})}(l)$ jumps discontinuously if the maxima leave the support and another segment contains the new maxima, compare Figure 7.

So far we have not discussed all boson propagators computed in the flow. The s -wave forward scattering boson propagators $K_{ss}^{(0)}$ and $K_{ss}^{(\hat{\pi})}$ and the s -wave superconducting boson propagators $D_{ss}^{(0)}$ and $D_{ss}^{(\hat{\pi})}$ cannot become singular since they are dominated by the initial local repulsion U . In Figure 9(b) their final values are plotted over hopping $-t'$. They are biggest in the crossover region between superconductivity and ferromagnetism, indicating the amount of screening and the low critical scale. The boson propagator $K_{11}^{(0)}$, representing a possible Pomeranchuk instability, is induced by magnetic correlations in the flow. However, it is not dominant in the parameter region considered here. The other boson propagators $D_{11}^{(\hat{\pi})}$, $M_{11}^{(0)}$, $M_{11}^{(\hat{\pi})}$, and $K_{11}^{(\hat{\pi})}$ remain smaller than 0.05 and hence are irrelevant here. Therefore, in order to further reduce computing cost, they could be omitted. In fact, only the boson propagators $D_{11}^{(\hat{\pi})}$, $M_{11}^{(\hat{\pi})}$, and $K_{11}^{(\hat{\pi})}$ do not satisfy the symmetry $B^{(a)}(l_x, l_y) = B^{(a)}(l_x, -l_y)$. If they are not computed in the flow, the angular segments only need to cover the interval $[0, \frac{\pi}{4}]$. This would halve the number of step functions necessary for the discretization of the momentum dependence described

in Section 7.

We have already mentioned that the effective on-site interaction changes although the initial on-site repulsion U of the Hubbard model is kept constant in the parametrization of the vertex function (9). Projecting to the on-site part gives the scale-dependent effective on-site coupling

$$U_{\text{eff}} = U + \int_{|l_x|+|l_y|\leq\pi} \frac{d^2\mathbf{l}}{(2\pi)^2} \sum_{a=0,\hat{\pi}} \left[-D_{\text{ss}}^{(a)}(\mathbf{l}) + \frac{3}{2}M_{\text{ss}}^{(a)}(\mathbf{l}) - \frac{1}{2}K_{\text{ss}}^{(a)}(\mathbf{l}) \right],$$

which is plotted in Figure 10 over hopping $-t'$. Although the critical scale is lowest in between the superconductor and the ferromagnet, the effective on-site coupling has not increased much in comparison to higher scales. This indicates that the amount of screening, especially in the crossover region between superconductivity and ferromagnetism, is substantial.

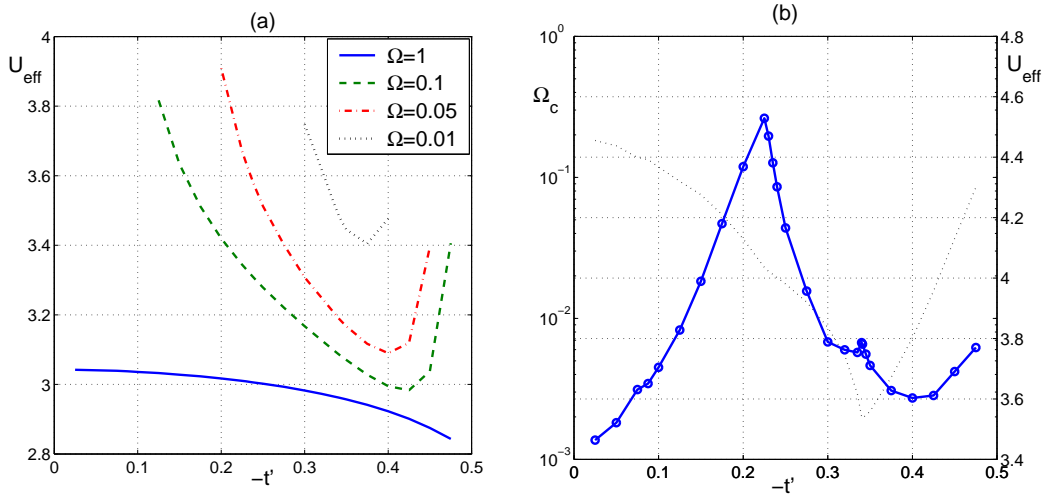


Figure 10: The effective on-site coupling U_{eff} is plotted in dependence of $-t'$ for different scales in (a). The curves to different values of Ω are drawn only over the interval where that Ω is still bigger than the critical scale Ω_c . In (b) U_{eff} is evaluated at the critical scale, which is plotted as a dotted line for comparison. The kinks in (b) indicate the crossovers of distinct instabilities.

In a second numerical computation we study the influence of offdiagonal boson propagators. In the superconducting channel we consider the boson propagators $D_{\text{ss}}^{(0)}$, $D_{\text{ss}}^{(\hat{\pi})}$, $D_{11}^{(0)}$, and $D_{1s}^{(0)}$. The first two are important to capture screening effects, the third describes $d_{x^2-y^2}$ superconductivity and the last is an offdiagonal boson propagator that couples s - and d -wave superconductivity. In the magnetic and forward scattering channel we only take into account the local s -wave boson propagators $M_{\text{ss}}^{(0)}$, $M_{\text{ss}}^{(\hat{\pi})}$, $K_{\text{ss}}^{(0)}$, and $K_{\text{ss}}^{(\hat{\pi})}$. Compared to the previous numerical calculation, apart from the irrelevant boson propagators $D_{11}^{(\hat{\pi})}$, $M_{11}^{(0)}$, $M_{11}^{(\hat{\pi})}$, and $K_{11}^{(\hat{\pi})}$, only the

boson propagator $K_{11}^{(0)}$, which indicates a possible Pomeranchuk instability, is omitted. However, $K_{11}^{(0)}$ remained relatively small in the first computation, see Figure 9. Note that for this choice of boson propagators there are no more offdiagonal terms than the one included.

The flow equations imply that the diagonal boson propagators obey the additional symmetry $B^{(a)}(l_x, l_y) = B^{(a)}(l_x, -l_y)$. The offdiagonal boson propagator $D_{1s}^{(0)}$ obeys this symmetry as well and is also symmetric under $\mathbf{l} \rightarrow -\mathbf{l}$. However, it is antisymmetric under exchange of $l_x \leftrightarrow l_y$. Therefore, compared to the choice of step functions described in Section 7, we only need to consider segments with an angle $\phi = \arctan \frac{l_y}{l_x}$ in the interval $[0, \frac{\pi}{4}]$. Since we still use the parameter values $m = 5$ and $n = 14$, the angular resolution is higher in this second numerical computation. Again we computed the RG flow of the boson propagators for coupling $U = 3$ at temperature zero and Van Hove filling for various $-t' \in (0, \frac{1}{2})$. Since no major process was omitted compared to the first numerical computation, no significant change could be observed in the figures presented. Furthermore, the maximum of the offdiagonal boson propagator $D_{1s}^{(0)}$ remains smaller than 0.3 for $-t' \geq 0.37$ and smaller than 0.03 for $-t' < 0.37$. The offdiagonal boson propagator that couples s - and d -wave superconductivity can therefore be neglected in good approximation.

The only difference in the two different numerical calculations is found in the shape of the antiferromagnetic boson propagator $M_{ss}^{(\hat{\pi})}$ for relatively high $-t'$. We already commented on the insufficient description of large radial momenta of the antiferromagnetic boson propagator $M_{ss}^{(\hat{\pi})}$, which is plotted in Figure 11 at $-t' = 0.3$ in dependence on ρ in different angular sectors, in (a) for the first and in (b) for the second numerical computation of this section. Note that the angular degeneracy in (a) is due to the same number of angular segments in the larger angular interval $[-\frac{\pi}{4}, \frac{\pi}{4}]$. The major difference between both figures is that in (b) the boson propagator has its maximal value at smaller radial momentum ρ . This can play a role in the search for an analytic parametrization of the antiferromagnetic boson propagator, although the plateau in the angular sector $\phi = 0$ for intermediate ρ seems to be its most important feature. However, note that the angle $\phi = 0$ is not a center of an angular sector in (b). The maximal value of the boson propagator is found in the nearest angular segment, which contains $\phi = 0$ but is centered at $\phi = \frac{\pi}{40}$. This could also be a partial explanation of the observed difference.

9 Conclusion

We have presented a novel parametrization of the one-loop one-particle irreducible RG equation for the four-point function and applied it to the two-dimensional Hubbard model using a novel RG regularization scheme. The parametrization is based on the idea to separate dominant interactions from irrelevant remainders, where the latter do not influence the leading instabilities of the flow. This idea is implemented by writing the effective two-fermion interaction as a sum of dominant terms

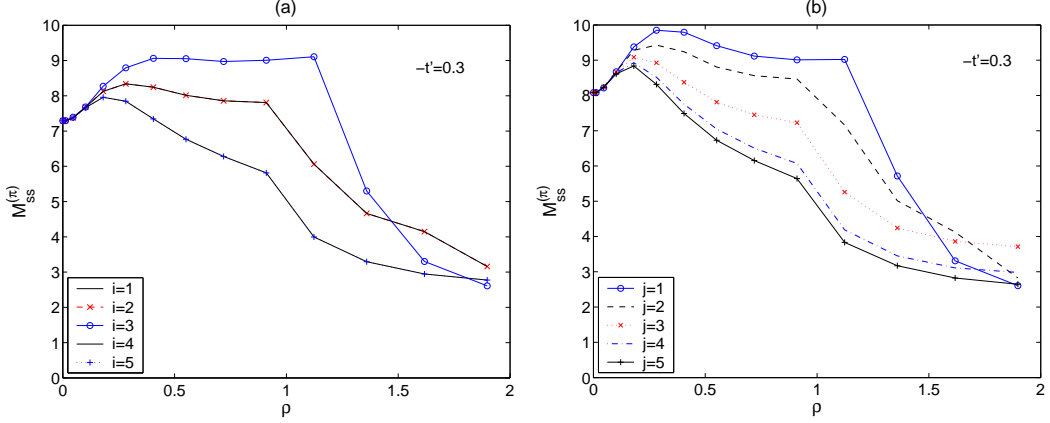


Figure 11: The antiferromagnetic boson propagator $M_{\text{SS}}^{(\hat{\pi})}$ plotted over radial momenta for different angular sectors centered at $\phi = \arctan \frac{l_y}{l_x}$. For the first numerical calculation shown in (a) the centers of the angular sectors take the values $\phi_i = -\frac{\pi}{4} + (i - \frac{1}{2})\frac{\pi}{10}$ and for the computation with an offdiagonal boson propagator in (b) the angular sectors are centered at $\phi_j = (j - \frac{1}{2})\frac{\pi}{20}$.

where fermion bilinears interact via exchange bosons. Each such term consists of a boson propagator and boson–two–fermion vertex functions. From the singular momentum structure of the RG equation we identify three different channels in the interaction. In these channels the boson–fermion vertex function is expanded in scale–independent form factors. We argued that only a few terms are needed in the expansions to describe the qualitative structure of the flow. The tails of the expansions are the above mentioned remainder terms, which are neglected. Although the scale dependent coefficient functions of the expansions are called boson propagators, they are kept as fermionic interaction terms. Their flow is computed by suitable projections of the fermionic RG equation.

The application of this method to the (t, t') –Hubbard model at Van Hove filling and temperature zero shows indeed that the essential qualitative structure of the one–loop RG is preserved. We are able to reproduce the leading weak coupling instabilities of the model, as they were found in previous RG studies using N –patch schemes. In particular, our results are in good qualitative agreement with the temperature RG flow [12]. We use a new frequency regularization, which like the temperature regularization does not artificially suppress ferromagnetism, but which allows to state the initial conditions of the RG flow more clearly. For an initial repulsive on–site interaction $U = 3$ we find three distinct regions, characterized by the leading weak coupling instability and depending on next to nearest neighbor hopping, see Figure 6. For small next to nearest neighbor hopping $-t'$ antiferromagnetism dominates. As was found in the N –patch schemes, antiferromagnetic correlations induce a $d_{x^2-y^2}$ –wave superconductivity instability, which becomes dominant for intermediate $-t'$. For high $-t'$ the leading instability is ferromagnetism. In

between the $d_{x^2-y^2}$ -wave superconducting and the ferromagnetic region the critical scale drops by two orders of magnitude. We argue that this is due to the mutual suppression of these opposing correlations. Compared to [12], however, we find that this suppression is weaker here. In particular, our result does not suggest a quantum critical point between the two regions. Because we have not been able to trace this discrepancy to certain scattering processes, we regard this matter as open and leave it for further study.

The proposed method is in general not restricted to temperature zero and Van Hove filling. Finite temperature only affects the calculation of the one-loop fermion bubbles, which then becomes more involved. Away from Van Hove filling triplet superconductivity plays a role for high $-t'$ [12]. The flow equations stated in Section 6 can account for that. However, it is not clear that a single form factor suffices to describe dominant triplet superconductivity. The results of [12] suggest that at least three different triplet form factors would have to be taken into account.

The benefit of the proposed parametrization of the vertex function is a reduction of the complexity of the full one-loop flow to some dominant terms. We believe that separating leading from subleading processes will help to gain further insight into the structure of the one-loop RG. However, we have not performed a detailed analysis of the remainder. The comparison with previous N -patch studies suggests, nevertheless, that we did capture the most important processes. A rigorous proof is particularly complicated at Van Hove filling due to the strong mixing of the particle-particle and the particle-hole channels. We gave clear arguments for determining the dominant terms in case of a regular and curved Fermi surface.

Practically, this reduction of complexity results in lower computing cost compared to previous N -patch schemes. In the numerical implementation the momentum dependence of the boson propagators is discretized using step functions. The choice of segments, where the step functions are constant, can be guided by the form of the one-loop bubbles. This allows a more precise discretization than the general patching of the vertex function in N -patch schemes. In particular, no momentum dependence is projected onto the Fermi surface. Furthermore, the proposed decomposition gives possibly way to further improvement. If the momentum dependence of the one-loop bubbles can be parameterized in an analytical form, then it should be possible to extract a functional parametrization of the boson propagators from the flow equations, at least for small momenta. Deviations for large momenta, away from the maxima of the boson propagators, could be subject to another negligible remainder. However, the momentum dependence of the bubbles is difficult to describe since a naive power expansion is not sufficient. Nevertheless, while in the numerical calculation we have neglected the frequency dependence of the boson propagators, a similar procedure for small frequencies could take into account at least part of the frequency dependence of the vertex function.

The proposed decomposition of the effective two-fermion interaction is of a form that suggests the decoupling of the fermion bilinears via multiple Hubbard Stratonovich transformations. The ambiguity of introducing boson fields is not

completely removed but at least reduced. This allows to continue the RG flow into the symmetry broken phase in a (partially) bosonized form.

We acknowledge financial support from DFG grant SA 1362/1–2 and DFG research group FOR 723.

References

- [1] P. B. Allen, *Fermi-surface harmonics: A general method for nonspherical problems. Application to Boltzmann and Eliashberg equations*, Phys. Rev. B **13** (1976), no. 4, 1416.
- [2] T. Baier, E. Bick, and C. Wetterich, *Temperature dependence of antiferromagnetic order in the Hubbard model*, Phys. Rev. B **70** (2004), 125111.
- [3] J. Feldman, J. Magnen, E. Trubowitz, and V. Rivasseau, *An Infinite Volume Expansion for Many Fermion Green's Functions*, Helv. Phys. Acta **65** (1992), 679.
- [4] N. Furukawa, T. M. Rice, and M. Salmhofer, *Truncation of a Two-Dimensional Fermi Surface due to Quasiparticle Gap Formation at the Saddle Points*, Phys. Rev. Lett. **81** (1998), no. 15, 3195.
- [5] R. Gersch, C. Honerkamp, and W. Metzner, *Superconductivity in the attractive Hubbard Model: functional renormalization group analysis*, New J. Phys. **10** (2008), 045003.
- [6] C. J. Halboth and W. Metzner, *d-Wave Superconductivity and Pomeranchuk Instability in the Two-Dimensional Hubbard Model*, Phys. Rev. Lett. **85** (2000), 5162.
- [7] C. J. Halboth and W. Metzner, *Renormalization group analysis of the two-dimensional Hubbard model*, Phys. Rev. B **61** (2000), 7364.
- [8] V. Hankevych, B. Kyung, and A.-M. S. Tremblay, *Weak ferromagnetism and other instabilities of the two-dimensional $t - t'$ Hubbard model at Van Hove fillings*, Phys. Rev. B **68** (2003), 214405.
- [9] C. Honerkamp, *Electron-doping versus hole-doping in the 2D t - t' Hubbard model*, Eur. Phys. J. B **21** (2001), 81.
- [10] C. Honerkamp, D. Rohe, S. Andergassen, and T. Enss, *Interaction flow method for many-fermion systems*, Phys. Rev. B **70** (2004), 235115.
- [11] C. Honerkamp and M. Salmhofer, *Magnetic and Superconducting Instabilities of the Hubbard Model at the Van Hove Filling*, Phys. Rev. Lett. **87** (2001), no. 18, 187004.

- [12] C. Honerkamp and M. Salmhofer, *Temperature-flow renormalization group and the competition between superconductivity and ferromagnetism*, Phys. Rev. B **64** (2001), 184516.
- [13] C. Honerkamp and M. Salmhofer, *Flow of the quasiparticle weight in the N -patch renormalization group scheme*, Phys. Rev. B **67** (2003), 174504.
- [14] C. Honerkamp and M. Salmhofer, *Eliashberg equations derived from the functional renormalization group*, Prog. Theor. Phys. **113** (2005), no. 6, 1145.
- [15] C. Honerkamp, M. Salmhofer, N. Furukawa, and T. M. Rice, *Breakdown of the Landau-Fermi liquid in two dimensions due to umklapp scattering*, Phys. Rev. B **63** (2001), 035109–1.
- [16] C. Karrasch, R. Hedden, R. Peters, Th. Pruschke, K. Schönhammer, and V. Meden, *A finite-frequency functional renormalization group approach to the single impurity Anderson model*, J. Phys.: Cond. Matt. **20** (2008), no. 34, 345205.
- [17] A. A. Katanin, *Fulfillment of Ward identities in the functional renormalization group approach*, Phys. Rev. B **70** (2004), 115109.
- [18] A. A. Katanin and A. P. Kampf, *Renormalization group analysis of magnetic and superconducting instabilities near van Hove band fillings*, Phys. Rev. B **68** (2003), 195101.
- [19] A. A. Katanin and A. P. Kampf, *Quasiparticle Anisotropy and Pseudogap Formation from the Weak-Coupling Renormalization Group Point of View*, Phys. Rev. Lett. **93** (2004), 106406.
- [20] H. C. Krahle, J. A. Müller, and C. Wetterich, *Generation of d -wave coupling in the two-dimensional Hubbard model from functional renormalization*, (2008), [arXiv:0801.1773v1](#).
- [21] W. A. de S. Pedra and M. Salmhofer, *Determinant Bounds and the Matsubara UV Problem of Many-Fermion Systems*, Comm. Math. Phys. **282** (2008), no. 3, 797.
- [22] J. Reiss, D. Rohe, and W. Metzner, *Renormalized mean-field analysis of anti-ferromagnetism and d -wave superconductivity in the two-dimensional Hubbard model*, Phys. Rev. B **75** (2007), 075110.
- [23] D. Rohe and W. Metzner, *Pseudogap at hot spots in the two-dimensional Hubbard model at weak coupling*, Phys. Rev. B **71** (2005), 115116.
- [24] M. Salmhofer, *Dynamical Adjustment of Propagators in Renormalization Group Flows*, Ann. Phys. (Leipzig) **16** (2007), no. 3, 171.

- [25] M. Salmhofer and C. Honerkamp, *Fermionic Renormalization Group Flows. Technique and Theory*, Prog. Theor. Phys. **105** (2001), no. 1, 1.
- [26] M. Salmhofer, C. Honerkamp, W. Metzner, and O. Lauscher, *Renormalization Group Flows into Phases with Broken Symmetry*, Prog. Theor. Phys. **112** (2004), no. 6, 943.
- [27] M. Salmhofer and C. Wiecekowsky, *Positivity and Convergence in Fermionic Quantum Field Theory*, J. Stat. Phys. **99** (2000), 557.
- [28] Manfred Salmhofer, *Renormalization. An Introduction*, Springer-Verlag, 1999.
- [29] F. Schütz, L. Bartosch, and P. Kopietz, *Collective fields in the functional renormalization group for fermions, Ward identities, and the exact solution of the Tomonaga-Luttinger model*, Phys. Rev. B **72** (2005), no. 3, 035107.
- [30] P. Strack, R. Gersch, and W. Metzner, *Renormalization group flow for fermionic superfluids at zero temperature*, (2008), [arXiv:0804.3994v1](#).
- [31] D. Zanchi, *Angle-resolved loss of Landau quasiparticles in 2D Hubbard model*, Europhys. Lett. **55** (2001), no. 3, 376.
- [32] D. Zanchi and H. J. Schulz, *Weakly correlated electrons on a square lattice: A renormalization group theory*, Europhys. Lett. **44** (1998), no. 2, 235.
- [33] D. Zanchi and H. J. Schulz, *Weakly correlated electrons on a square lattice: Renormalization-group theory*, Phys. Rev. B **61** (2000), no. 20, 13609.